ANL-HEP-PR-95-36

December 15, 1995

# Analytic Calculation of Prompt Photon plus Associated Heavy Flavor at Next-to-Leading Order in QCD

Edmond L. Berger and L. E. Gordon

*High Energy Physics Division, Argonne National Laboratory, Argonne, IL 60439*

## Abstract

Contributions through second order, $O(\alpha_s^2)$, in perturbative quantum chromodynamics are calculated analytically for inclusive associated production of a prompt photon and a charm quark at large values of transverse momentum in high energy hadron-hadron collisions. Seven partonic subprocesses contribute at order $\alpha_s^2$. We find important corrections to the lowest order, $O(\alpha_s)$, subprocess $cg \to \gamma c$. We demonstrate to what extent data from $p + \bar{p} \to \gamma + c + X$ may serve to measure the charm quark density in the nucleon.

## I. INTRODUCTION

Because photons couple in point-like fashion to quarks, observation, among the final-state particles in a high energy collision, of photons carrying large values of transverse momentum provides an incisive probe of the short distance hadron dynamics of the collision. This fact explains the substantial theoretical and experimental interest shown in studies of the cross section for production of photons at large angles in hadron-hadron and lepton-hadron scattering and in electron-positron annihilation processes. At stake are precise tests of the theory of perturbative quantum chromodynamics (QCD) and use of data to determine properties of the relativistic proton such as the momentum distribution of its constituent gluons and quarks. Discovery of the charm quark and, later, of the bottom quark stimulated interest in the dynamics of their relatively copious production in high energy interactions of hadrons. Recent experimental advances now offer the possibility of studies of the associated production of a photon ($\gamma$) carrying large transverse momentum along with a heavy quark ($Q$) whose transverse momentum balances a substantial portion of that of the photon. [1] In this paper, we report a fully analytic next-to-leading order QCD calculation of the two-particle inclusive distribution for prompt photon plus associated heavy flavor production at large values of transverse momentum, with specification of the momentum variables of both the final prompt photon and the final heavy quark. These results should facilitate further experimental tests of correlations inherent in the QCD matrix elements and provide a means for measuring the charm quark density in the nucleon.

Although a qualitative description may be obtained from lowest-order perturbation theory, more precise predictions of the momentum distribution for the inclusive production a heavy quark (or antiquark) require perturbative calculations that extend to higher order. [2] Likewise, perturbative QCD calculations of inclusive and isolated prompt single photon production are available. [3–5] At the level of two-particle inclusive final states, next-to-leading order QCD calculations have been done for $\gamma\gamma$ production [6,7], for $\gamma$-hadron production [8] and for $\bar{Q}Q$ correlations. [9] The cross section for the production of two hadronic jets has

been studied at $O(\alpha_s^3)$ by several authors. [10] Constraints on the charm and strange quark densities from data on intermediate vector-boson production are discussed in Ref. [11].

For values of transverse momentum $p_T^Q$ of the heavy quark significantly larger than the mass $m_Q$ of the heavy quark, the cross section for the two-particle inclusive reaction $p + \bar{p} \to \gamma + Q + X$ may be calculated from the leading order QCD subprocess, the quark-gluon Compton process, $g + Q \to \gamma + Q$. This subprocess is of first order in the strong coupling strength $\alpha_s$. The cross section is obtained as a convolution of the hard-scattering QCD matrix with probability distributions that specify the initial gluon and heavy quark constituent momentum densities in the incident hadrons, $p$ and $\bar{p}$. At next-to-leading order in QCD, several subprocesses contribute to the $\gamma + Q$ final state:

$$g + Q \to g + Q + \gamma \tag{1.1a}$$

$$g + g \to Q + \bar{Q} + \gamma \tag{1.1b}$$

$$q + \bar{q} \to Q + \bar{Q} + \gamma \tag{1.1c}$$

$$q + Q \to q + Q + \gamma \tag{1.1d}$$

$$\bar{q} + Q \to \bar{q} + Q + \gamma \tag{1.1e}$$

$$Q + \bar{Q} \to Q + \bar{Q} + \gamma \tag{1.1f}$$

$$Q + Q \to Q + Q + \gamma \tag{1.1g}$$

For computation of the cross section for $\bar{Q}$ production, the set of next-to-leading order subprocesses is obtained from those of Eq. (1.1) after replacement of the initial $Q's$ by $\bar{Q}'s$ in Eqs. (1.1a), (1.1d), (1.1e), (1.1g). We note that for values of $p_T^Q$ that are comparable to or less than $m_Q$ there would be no $O(\alpha_s)$ subprocess, and the proper hard scattering expansion would entail only the subprocesses of Eqs. (1.1b) and (1.1c). For the remainder of this paper, we limit ourselves to charm production, and we work with the massless Q approximation, $m_c = 0$.

We are interested ultimately in the fully differential two-particle inclusive cross section, $E_\gamma E_Q d\sigma/d^3p_\gamma d^3p_Q$, where $(E, p)$ represents the four-vector momentum of the $\gamma$ or $Q$. For

each subprocess listed in Eq. (1.1), this calculation requires integration of the momentum of the unobserved final parton ($g$, $\bar{Q}, q$, or $\bar{q}$) and over the initial parton momentum densities. Collinear singularities are handled analytically by dimensional regularization and absorbed into initial-state parton momentum densities or final-state fragmentation functions. To make the analytic calculation tractable, we chose to work in terms of the transverse momentum of the final $\gamma$, $p_T^\gamma$, and the ratio of the heavy quark and photon transverse momenta:

$$z = -\frac{p_T^Q . p_T^\gamma}{(p_T^\gamma)^2}. \tag{1.2}$$

To warrant use of perturbation theory (and the massless $Q$ approximation), we limit our considerations to $z > 0$ and $p_T^\gamma > 10$ GeV. The results should be applicable quantitatively for $p_T^c \gg m_c$. The distribution in $z$ from the leading order subprocess $g + Q \to \gamma + Q$ is peaked sharply at $z = 1$ (a $\delta(1 - z)$ function in the naive collinear initial parton approximation). The next-to-leading order processes alter the size of this sharp peak and produce a broad distribution above and below $z = 1$.

Contributions to hard photon production from long-distance quark to photon and gluon to photon fragmentation processes have been emphasized theoretically, [12] parametrized phenomenologically in leading order, [13] and evolved in next-to-leading order. [14,15] These terms may account for more than half of the calculated inclusive single photon cross section at modest values of transverse momentum at the Fermilab Tevatron collider. Because of our kinematic restriction $z > 0$, there will be no contributions to the final cross section from $Q \to \gamma$ fragmentation, where $Q$ is the observed quark/anti-quark, from among the subprocesses in Eq. (1.1). On the other hand, fragmentation of the unobserved final parton into a photon in subprocesses (1.a-g) will contribute to the cross section and produce photons that carry $p_T$ less than that of $p_T^Q$, mostly populating the region $z > 1$. Photons originating through fragmentation are likely to emerge in the neighborhood of associated hadrons. An experimental isolation restriction is needed before a clean identification can be made of the photon and a measurement made of its momentum. Isolation reduces the size of the observed fragmentation contribution. To represent the effects of isolation, we

should use fragmentation functions defined with a cone size. Photon isolation complicates the theoretical interpretation of results, however, since it threatens to upset the cancellation of infra-red divergences in perturbation theory. [5] In this paper, we calculate the contributions from photon fragmentation at leading order only, and, except for one illustrative figure, we neglect the isolation requirements.

After integration over the longitudinal momentum of the heavy quark, we present our results in terms of the cross section $d\sigma/dp_T^\gamma dy^\gamma dz$. Here, $y^\gamma$ represents the rapidity of the $\gamma$. Our desire to perform a fully analytic calculation restricts our ability to provide a more differential cross section in this paper (i.e., a cross section also differential in $y^Q$). In a later more detailed paper, we will present such results obtained from a versatile combination of analytic and Monte Carlo techniques. [16] In that method, selections may be made on several variables and photon isolation restrictions are easier to impose. An earlier theoretical paper addresses prompt photon plus associated charm production at large values of transverse momentum, as we do here, but our analysis differs from that of Ref. [17]. The calculation of the photon-plus-charm cross section in Ref. [17] is done in lowest order while ours is done at next-to-leading order. In lowest order, the subprocesses $gg \to \gamma c\bar{c}$ and $q\bar{q} \to \gamma c\bar{c}$ contribute in the massive case, whereas $cg \to \gamma c$ plus fragmentation processes contribute in the massless case. In a forthcoming paper, we intend to examine the massive case in detail and to discuss comparisons with the massless case in the regions of phase space of their respective applicability. As remarked above, our massless approach should be appropriate and applicable in the domain in which there is effectively only one large scale, $p_T^c \gg m_c$.

For the interval in $p_T^\gamma$ of current experimental interest, 10 GeV $< p_T^\gamma <$ 50 GeV, the $gc$ and $gg$ subprocesses of Eqs. (1.1a) and (1.1b) are the most important quantitatively at Fermilab Tevatron energies, owing to the strength of the gluon density. For $p_T^\gamma > 70$ GeV, calculations of the inclusive yield of single photons indicate that the $q\bar{q}$ subprocess begins to dominate, but the cross section is small in this region. Dominance of the perturbative subprocess initiated by $gc$ scattering is preserved after the next-to-leading terms are included, justifying use of data from $p + \bar{p} \to \gamma + c + X$ in attempts to measure the charm quark

momentum density in the nucleon. However, we show that other subprocesses account for about 50% of the cross section at currently accessible values of $p_T^\gamma$. The "background" associated with these subprocesses must be taken into account in analyses done to extract the charm density.

Our results are provided in terms of the momentum of the charm quark. In a typical experiment, [1] the momentum of the quark may be inferred from the momentum of prompt lepton decay products or the momentum of charm mesons, such as $D^*$'s. Alternatively, our distributions in $z$ or $p_T^c$ may be convoluted with charm quark fragmentation functions, deduced from, e.g., $e^+e^-$ annihilation data, to provide distributions for the prompt leptons or $D^*$'s.

In Sec. II, we present our analysis of the leading and next-to-leading order contributions to the partonic hard-scattering cross sections. Numerical results are described in Sec. III, and a summary of our conclusions is provided in Sec. IV. An Appendix is included in which we present our method for performing the required three-particle final-state integrals in n-dimensions to extract the singularities of the two-particle inclusive hard cross section.

## II. ANALYTICAL CALCULATION

We consider the two particle inclusive reaction $A+B \to \gamma+c+X$ where $A$ and $B$ denote incident hadrons; $p^\gamma$ and $p^c$ denote the four-vector momenta of the photon and charm quark. The usual Mandelstam invariants are defined in terms of the momenta of the two incoming hadrons $P_A$ and $P_B$, and the momentum fractions of the initial partons, $x_1$ and $x_2$, via

$$\begin{aligned} \hat{s} &= (x_1 P_A + x_2 P_B)^2 = x_1 x_2 s \\ \hat{t} &= (x_1 P_A - p^\gamma)^2 \\ \hat{u} &= (x_2 P_B - p^\gamma)^2. \end{aligned} \tag{2.1}$$

Here $\sqrt{s}$ is the center-of-mass energy in the hadronic system. We define

$$v = 1 + \frac{\hat{t}}{\hat{s}}$$

$$w = \frac{-\hat{u}}{\hat{s}+\hat{t}}. \tag{2.2}$$

### A. Leading Order Contributions

In leading order in perturbative QCD, only one direct subprocess contributes to the hard-scattering cross section, the QCD Compton process $cg \to \gamma c$, unlike the case for single inclusive prompt photon production, where the annihilation process $q\bar{q} \to \gamma g$ also contributes. Since the leading order direct partonic subprocess has a two-body final state, the photon and $c$-quark are produced with balancing transverse momenta, and the variable $z$, defined in Eq. (1.2), is always unity.

The leading order direct partonic cross section is

$$\frac{d\hat{\sigma}}{dvdzdw} = \frac{d\hat{\sigma}}{dv}\delta(1-z)\delta(1-w), \tag{2.3}$$

where $d\hat{\sigma}/dv$ is the partonic Born cross section:

$$\frac{d\hat{\sigma}}{dv}(cg \to \gamma c) = \frac{1}{N_C}\frac{\pi\alpha_{em}\alpha_s e_q^2}{\hat{s}}\frac{1+(1-v)^2}{1-v}. \tag{2.4}$$

Here $\alpha_{em}$ and $\alpha_s$ are the electromagnetic and strong coupling constants, respectively, $N_C = 3$ is the number of colors, and $e_q$ denotes the quark charge.

The full expression for the physical cross section in leading order is

$$\frac{d\sigma}{dp_T^\gamma dy^\gamma dz} = 2\pi p_T^\gamma \frac{1}{\pi s}\int_{VW}^1 \frac{dv}{1-v} f_g^A(x_1, M^2) f_c^B(x_2, M^2)\frac{d\hat{\sigma}}{dv}\delta(1-z)\delta(1-w) + (c \leftrightarrow g). \tag{2.5}$$

Quantities $V$ and $W$ are defined similarly to $v$ and $w$, Eq. (2.2), but in the hadronic system; $f^A(x_1, M^2)$ denotes the parton density in hadron $A$ as a function of the momentum fraction $x_1$ and factorization scale $M$.

In addition to the lowest order direct subprocess just discussed, $cg \to \gamma c$, there are fragmentation contributions that are also effectively of leading order in $\alpha_s$. In these contributions the photon is produced through fragmentation of a final-state parton from any of

the $O(\alpha_s^2)$ subprocesses listed below. The fragmentation functions are essentially of order $O(\alpha_{em}/\alpha_s)$

$$\begin{aligned} c + g &\to g + c \\ g + g &\to c + \bar{c} \\ c + q &\to c + q \\ c + \bar{q} &\to c + \bar{q} \\ c + c &\to c + c \\ c + \bar{c} &\to c + \bar{c} \\ q + \bar{q} &\to c + \bar{c}. \end{aligned} \tag{2.6}$$

We are interested in configurations in which the photon and charm quark have relatively large and to-some-extent balancing values of transverse momentum. Therefore, in the cases of the first, third, and fourth of the subprocesses listed above, the photon is produced from fragmentation of the $g$ and non-charm quark $q$, respectively. In the other cases it is produced in the fragmentation of one of the (anti)charm quarks. The expression we use to evaluate the fragmentation contributions is

$$\begin{aligned} \frac{d\sigma}{dp_T^\gamma dy^\gamma dz} = 2\pi p_T^\gamma \frac{1}{\pi s} \int_{1-V+VW}^1 \frac{dz'}{z'^2} \int_{VW}^1 \frac{dv}{1-v} f_a^A(x_1, M^2) f_b^B(x_2, M^2) \frac{d\hat{\sigma}^{ab\to iX}}{dv} \\ \times D_{\gamma/i}(z', Q^2) \delta(\frac{1}{z} - z'). \end{aligned} \tag{2.7}$$

In a fully consistent next-to-leading calculation, one should calculate the subprocesses in Eq. (2.6) to $O(\alpha_s^3)$, since the photon fragmentation functions that are convoluted with the hard subprocess cross sections are of $O(\alpha_{em}/\alpha_s)$. For simplicity, we include them in $O(\alpha_s^2)$ only. In fact, next-to-leading order fragmentation contributions to single prompt photon production have been included only once before [4]. We expect the next-to-leading order corrections to the fragmentation contributions to be insignificant numerically especially after isolation cuts are imposed.

### B. Next-to-leading order Contributions

There are two classes of contributions in next-to-leading order. First there are the virtual gluon exchange corrections to the lowest order process. Examples are shown in Fig.1b. These amplitudes interfere with the Born amplitudes and contribute at $O(\alpha_{em}\alpha_s^2)$. They have been calculated twice before. [3,4] We use the results of Ref. [4]. The virtual contributions are proportional to $\delta(1-z)$ and $\delta(1-w)$. At next-to-leading order there are also three-body final-state contributions, listed in Eq. (1.1). The matrix elements for these are also taken from Ref. [4], where they are calculated for single inclusive prompt photon production.

The main task of our calculation is to integrate the three-body matrix elements over the phase space of the unobserved particle in the final state. The situation here is different from the standard case of single inclusive particle production, first developed in Ref. [18], since we wish to retain as much control as possible over the kinematic variables of a second particle in the final state, while at the same time integrating over enough of the phase space to ensure cancellation of all infrared and collinear divergences, inherent when massless particles are assumed. Because our goal is to provide a fully analytic calculation, we find it necessary to integrate over the full range of rapidity of one of the observed final-state particles. We choose to integrate over that of the charm quark, since the photon is usually considered the trigger particle in the experiments.

The situation here is similar to that met by Aurenche *et al* [6,8], and we use a similar technique to perform the phase space integrals. We give a fairly detailed outline of the method since it is necessary to adapt it to our situation and also because it has not been widely used. We believe our presentation clarifies certain details which are not stressed in the above references.

The three-body phase space integration is done in the rest frame of the observed $c$ (or $\bar{c}$-quark) and the third unobserved parton. Denoting the momenta of the process by $p_1 + p_2 \to k_1 + k_2 + k_3$, we work in the rest frame of $k_2$ and $k_3$, where $k_1$ is the momentum of the trigger photon. The final form of the three-particle phase space integral (see the

Appendix) is

$$PS^{(3)} = \frac{\pi\hat{s}}{8(2\pi)^5}\left(\frac{4\pi}{\hat{s}}\right)^{\epsilon}\frac{v}{\Gamma(1-2\epsilon)}\left(\frac{4\pi}{\hat{s}wv(1-v)}\right)^{\epsilon}v^{-\epsilon}(1-w)^{-\epsilon}2\sqrt{\frac{w(1-v)}{(1-vw)}}$$
$$\times\left[\frac{1-w+4w(1-v)z(1-z)}{1-vw}\right]^{-\epsilon}\int_0^{\pi}d\theta_2\sin^{-2\epsilon}(\theta_2). \tag{2.8}$$

We are left to perform the final integration of the squared matrix elements over $\theta_2$.

As in the case of single inclusive cross section calculations, documented extensively elsewhere, one can use relations among the Mandelstam variables to reduce complex combinations of them to simple products and ratios. The phase space integral over $\theta_2$ is performed in $4-2\epsilon$ dimensions, thereby exposing collinear and soft singularities as poles in $\epsilon$. After the three-particle phase space integrals are performed, we obtain a three-body final state hard-scattering cross section that we represent by the expression

$$\frac{d\sigma_{ij}^R}{dvdwdz}\left(\hat{s},v,w,z,\frac{1}{\epsilon^2},\frac{1}{\epsilon}\right).$$

Superscript $R$ indicates that this is the subprocess cross section for a real three-body final-state contribution, as distinct from the contribution from the virtual gluon exchange contributions that we denote $\sigma_{ij}^V$. The subscripts $ij$ designate one of the processes in Eq. (1.1). In general, $\sigma_{ij}^R$ has single and double poles in $\epsilon$. In accord with the factorization theorem of perturbative QCD, the double and some of the single poles cancel between the real and virtual contributions. The remaining single poles in $\epsilon$ represent collinear divergences that are subtracted into parton densities and fragmentation functions.

In order to illustrate how the collinear singularities are handled we discuss a few representative examples.

(a) $c+g\to\gamma+c+X$

This is the QCD Compton process plus higher order corrections. We label the momenta by

$$c(p_1)+g(p_2)\to\gamma(k_1)+c(k_2)+g(k_3). \tag{2.9}$$

In performing the phase space integration, we expect to encounter singularities where the gluon $k_3$ becomes soft and/or parallel to $p_1, p_2$ or $k_2$. Since we require that the observed charm quark and $\gamma$ be in opposite hemispheres, we will not encounter any singularity where $k_1$ and $k_2$ are collinear (see the Appendix). In the cases where the gluon is either soft and/or parallel to $p_1$ or $p_2$, then $z = 1$. We expose the $z \to 1$ singularities by using the expansion

$$\frac{1}{|1-z|^{1+2\epsilon}} = \frac{1}{-2\epsilon}\delta(1-z) + \frac{\theta(1-z)}{(1-z)_+} + \frac{\theta(z-1)}{(z-1)_+} - 2\epsilon \left(\frac{\ln(1-z)}{1-z}\right)_+ \theta(1-z) + O(\epsilon^2). \tag{2.10}$$

There are plus-distributions in the variable $z$, as well as the usual ones in $w$ that arise in the single particle inclusive case and correspond to the gluon becoming either soft or collinear to $k_2$. Plus-distributions in $z$ and $w$ can be encountered simultaneously and must be treated carefully in the numerical evaluation of the cross section.

Once the phase space integrals are performed and the soft and collinear poles are exposed, we can add the real three-body contributions to the virtual gluon exchange terms, after which all the double poles cancel along with some single poles. The remaining collinear poles must be factored into the parton distribution and fragmentation functions. We perform these subtractions in the universal or $\overline{MS}$ scheme, described in detail in many places.

To account for all collinear configurations allowed in the subprocess, the counter cross section or factorization formula that must be added to our results in order to cancel the collinear poles is

$$\begin{aligned}\frac{1}{\hat{s}v}\frac{d\sigma^F}{dvdwdz} = -\frac{\alpha_s}{2\pi}\Bigg[&\frac{1}{\hat{s}v}H_{cc}(w, M^2)\frac{d\sigma^{cg\to\gamma c}}{dv}(w\hat{s}, v, \epsilon)\delta(1-z) \\ &+ \frac{1}{\hat{s}(1-vw)}H_{gg}\left(\frac{1-v}{1-vw}, M^2\right)\frac{d\sigma^{cg\to\gamma c}}{dv}(w\hat{s}, vw, \epsilon)\delta(1-z) \\ &+ \frac{1}{\hat{s}v}\tilde{H}_{cc}(z, M''^2)\frac{d\sigma^{cg\to\gamma c}}{dv}(\hat{s}, v, \epsilon)\theta(1-z)\delta(1-w)\Bigg].\end{aligned} \tag{2.11}$$

$$H_{ij}(z, Q^2) = -\frac{1}{\hat{\epsilon}}P_{ij}(z)\left[\frac{\mu^2}{Q^2}\right]^{\epsilon} + f_{ij}(z), \tag{2.12}$$

and

$$\tilde{H}_{ij}(z,Q^2) = -\frac{1}{\hat{\epsilon}} P_{ij}(z) \left[\frac{\mu^2}{Q^2}\right]^{\epsilon} + d_{ij}(z). \tag{2.13}$$

Functions $P_{ij}(z)$ are the one-loop splitting functions [18], $f_{ij}(z) = 0$ and $d_{ij}(z) = 0$ in the $\overline{MS}$ factorization scheme, and $\mu$ is the renormalization scale. In the $\overline{MS}$ scheme, $1/\hat{\epsilon} \equiv 1/\epsilon - \gamma_E + \ln 4\pi$.

In Eq. (2.11), we distinguish the factorization scale $M$ and the quark to quark plus gluon fragmentation scale $M''$. The last term indicates that we factor the collinear singularity that arises when the observed charm quark $k_2$ becomes parallel to the gluon, $k_3$, into a fragmentation function at scale $M''^2$, for the production of a charm quark. Note that this singularity occurs in the region $z \leq 1$, since the photon must balance the momentum of the charm-gluon system.

We are free to convolute our cross section with a fragmentation function that describes the formation of specific charm decay products (e.g., D or D$^*$ mesons), but we choose not to do so in this paper.

(b) $g + g \to \gamma + c + \bar{c}$

In the gluon-gluon fusion process, $gg \to \gamma c\bar{c}$, the photon may become collinear to the unobserved final-state quark, a situation not encountered in the $gc$ process discussed above. This singularity occurs at $z = z_1$ where $z_1 = 1/(1 - v + vw)$, and, as discussed in the Appendix, we use an expansion similar to that in Eq. (2.10) to expose the singularity. Note that this singularity occurs in the region $z \geq 1$, and that $z$ is exactly the reciprocal of the usual fragmentation variable for a parton to fragment into a particle with a fraction of its momentum, $1/z$. The factorization formula for this process is

$$\begin{aligned}\frac{1}{\hat{s}v}\frac{d\sigma^F}{dvdwdz} = -\frac{\alpha_s}{2\pi}\Bigg[&\frac{1}{\hat{s}v} H_{cg}(w, M^2) \frac{d\sigma^{cg\to\gamma c}}{dv}(w\hat{s}, v, \epsilon)\delta(1-z) \\ &+ \frac{1}{\hat{s}(1-vw)} H_{cg}\left(\frac{1-v}{1-vw}, M^2\right) \frac{d\sigma^{gc\to\gamma c}}{dv}(w\hat{s}, vw, \epsilon)\delta(1-z) \\ &+ \frac{1}{\hat{s}(1-v+vw)} \tilde{H}_{\gamma\bar{c}}(1-v+vw, M'^2) \frac{d\sigma^{gg\to c\bar{c}}}{dv}(\hat{s}, \frac{vw}{1-v+vw}, \epsilon)\delta(z_1 - z)\Bigg].\end{aligned} \tag{2.14}$$

In this equation, we distinguish the factorization scale $M$ and the quark to photon fragmentation scale $M'$.

(c) $q + \bar{q} \to \gamma + c + \bar{c}$

The process $q\bar{q} \to \gamma c\bar{c}$, as well as that of Eq. (1.1f), has a final-state collinear singularity when a gluon splits into a collinear $c\bar{c}$ pair, and, in addition, a singularity when the photon is produced from fragmentation of a final-state quark. The factorization formula for this case is

$$\begin{aligned}\frac{1}{\hat{s}v}\frac{d\sigma^F}{dvdwdz} = -\frac{\alpha_s}{2\pi}\Bigg[&\frac{1}{\hat{s}v}\tilde{H}_{cg}(z, M''^2)\frac{d\sigma^{q\bar{q}\to\gamma g}}{dv}(\hat{s}, v, \epsilon)\theta(1-z) \\ &+ \frac{1}{\hat{s}(1-v+vw)}\tilde{H}_{\gamma\bar{c}}(1-v+vw, M'^2)\frac{d\sigma^{q\bar{q}\to c\bar{c}}}{dv}(\hat{s}, \frac{vw}{1-v+vw}, \epsilon) \\ &\times \delta(z_1 - z)\Bigg]. \end{aligned} \tag{2.15}$$

### C. Physical cross section

Once all singularities are dealt with, we calculate the physical cross section by convoluting the hard partonic cross section with parton distribution functions. In terms of the variables we are using, the cross section at next-to-leading order is

$$\begin{aligned}\frac{d\sigma}{dp_T^\gamma dy^\gamma dz} = 2\pi p_T^\gamma \frac{1}{\pi s}\sum_{i,j}\int_{VW}^1 \frac{dv}{1-v}\int_{VW/v}^1 \frac{dw}{w} f_i^A(x_1, M^2) f_j^B(x_2, M^2) \\ \left[\frac{1}{v}\frac{d\hat{\sigma}^{ij}}{dv}\delta(1-z)\delta(1-w) + \frac{\alpha_s(\mu^2)}{2\pi}K_{ij}(\hat{s}, v, w, z, \mu^2, M^2, M'^2, M''^2)\right]. \end{aligned} \tag{2.16}$$

The first term within the square brackets is the leading order part, and

$$K_{ij}(\hat{s}, v, w, z, \mu^2, M^2, M'^2, M''^2)$$

is the next-to-leading order correction term; $K_{ij}$ may include virtual gluon exchange contributions.

Taking the $cg$ subprocess as an example, we outline how we obtain the function $K_{ij}(\hat{s}, v, w, z, \mu^2, M^2, M'^2, M''^2)$. The virtual gluon exchange contributions are represented by

$$\frac{d\sigma_{cg}^V}{dvdwdz}\left(\hat{s}, v, \mu^2, \frac{1}{\epsilon^2}, \frac{1}{\epsilon}\right).$$

They are proportional to $\delta(1-w)$ and $\delta(1-z)$. The real three-body contributions are denoted

$$\frac{d\sigma_{cg}^{R}}{dvdwdz}\left(\hat{s},v,w,z,\frac{1}{\epsilon^2},\frac{1}{\epsilon}\right).$$

Combining the three-body final-state contribution and the virtual gluon exchange contribution and adding to these the subtraction term in Eq. (2.11), we derive a finite subprocess cross section:

$$\begin{aligned}K_{cg}(\hat{s},v,w,z,\mu^2,M^2,M''^2) = &\frac{d\sigma_{cg}^{V}}{dvdwdz}\left(\hat{s},v,\mu^2,\frac{1}{\epsilon^2},\frac{1}{\epsilon}\right)+\\ &\frac{d\sigma_{cg}^{R}}{dvdwdz}\left(\hat{s},v,w,z,\frac{1}{\epsilon^2},\frac{1}{\epsilon}\right)+\\ &\frac{d\sigma_{cg}^{F}}{dvdwdz}\left(\hat{s},v,w,z,\frac{1}{\epsilon},M^2,M''^2\right).\end{aligned} \tag{2.17}$$

At this stage all single and double poles cancel, and we are left with a finite cross section dependent on the factorization scale $M$ and fragmentation scale $M''$. Because of the additional variable $z$, the function $K_{cg}$ is quite lengthy when compared to that for inclusive single photon production. [4] In schematic notation, where only the $z$-distributions are made explicit, we can write the hard-scattering cross section as

$$\begin{aligned}K_{cg}(\hat{s},v,w,z,\mu^2,M^2,M''^2) = &\, c_1(v,w)\delta(1-z)+c_2(v,w)\frac{\theta(1-z)}{(1-z)_+}\\ &+c_3(v,w)\frac{\theta(z-1)}{(z-1)_+}+c_4(v,w)\left(\frac{\ln(1-z)}{1-z}\right)_+\\ &+c_5(v,w,z).\end{aligned} \tag{2.18}$$

The functions $c_i(v,w)$ contain, in general, distributions in $(1-w)$, and they can be expressed by

$$\begin{aligned}c_i(v,w) = &\, c_i^1(v)\delta(1-w)+c_i^2(v)\frac{1}{(1-w)_+}+c_i^3(v)\left(\frac{\ln(1-w)}{1-w}\right)_+\\ &+c_i^4(v,w).\end{aligned} \tag{2.19}$$

Similar expressions can be written for the other subprocesses. These will generally involve the fragmentation scale on the photon leg, $M'$, and additional distributions in $(z_1-z)$ and

$(z - z_1)$. These are defined as normal plus-distributions, but in the intervals $[0, z_1]$, and $[z_1, z_{max}]$ , respectively. We integrate the distributions between limits other than these. For example, if the limits in the first case are $[z_a, z_1]$, we must make the replacement

$$\frac{1}{(z_1 - z)_+} = \frac{1}{(z_1 - z)_{z_a}} + \delta(z_1 - z) \ln(z_1 - z_a), \tag{2.20}$$

where the new distribution is defined by

$$\int_{z_a}^{z_1} dz \frac{f(z)}{(z_1 - z)_{z_a}} = \int_{z_a}^{z_1} dz \frac{f(z) - f(z_1)}{z_1 - z}. \tag{2.21}$$

By expanding our integrated matrix elements as plus-distributions in $z$, we are able to expose the singularities that occur at $z = 1$ and $z = z_1$. This procedure ensures that these integrable singularities can be treated numerically. However, it also means that our analytic distributions in z are singular at $z = 1$ and $z = z_1$. For comparison with experiment, we provide predictions for the $z$ dependence in the form of histograms with finite bin-widths $\Delta z$, reminiscent of experimental resolution. As in Ref. [6], we define

$$\frac{d\sigma}{dp_T^\gamma dy^\gamma dz} = \frac{1}{\Delta z} \int_{z - \frac{\Delta z}{2}}^{z + \frac{\Delta z}{2}} \frac{d\sigma}{dp_T^\gamma dy^\gamma dz'} dz'. \tag{2.22}$$

For distributions in $p_T^\gamma$, we integrate over a specified range of $z$,

$$\frac{d\sigma}{dp_T^\gamma dy^\gamma} = \int_{z_a}^{z_b} \frac{d\sigma}{dp_T^\gamma dy^\gamma dz} dz. \tag{2.23}$$

This completes our discussion of the calculation. Further details can be found in the Appendix.

## III. NUMERICAL RESULTS AND DISCUSSION

In this section we present and discuss explicit evaluations of the correlated production cross section of charm plus a prompt photon. We provide results at $\bar{p}p$ center-of-mass energy $\sqrt{s} = 1.8$ TeV appropriate for the CDF and D0 experimental investigations underway at Fermilab. The cross sections we evaluate are those derived in the text: Eqs. (2.5), (2.7) and

(2.16). For the electromagnetic coupling strength we use $\alpha_{em} = 1/137$, and we employ a two-loop expression for $\alpha_s(\mu^2)$ with quark threshold effects handled properly. We choose identical values for the renormalization, factorization, and fragmentation scales, $\mu = M = M' = M''$. In the results presented below, we vary $\mu$ to examine the sensitivity of the cross section to its choice. We choose $\Lambda^{(4)}_{QCD}$ according to the parton distribution set we use; $\Lambda^{(4)}_{QCD} = 0.200$ for the GRV parton distributions. [20] The sums run over 4 flavors of quarks $(u, d, c, s)$, all assumed massless. We do not include a $b$ quark contribution in our calculation.

Most of the calculations reported here are done with the GRV parton densities [20]. We observe some differences when we use instead the CTEQ3M densities [21]. The magnitude and Bjorken $x$ dependence of the charm quark density in these two sets are similar, as shown in Fig. 2, but show some differences at large $x$, leading to a 30% difference in the cross section at $p_T^\gamma = 60GeV$. In these densities, the charm quark probability is generated through perturbative evolution, and there is no non-perturbative intrinsic charm [22] component. Neither density may be correct since there is little direct experimental information to constrain this density [11]. A goal of our analysis is to ascertain the extent to which the $gc$ initial state is expected to dominate the cross section for $p + \bar{p} \to \gamma + c + X$, and, thus, the extent to which data from this reaction may serve to measure the charm quark density.

The quark-to-photon fragmentation function is expressed as

$$z\, D_{q\to\gamma}(z,\mu^2) = \frac{\alpha_{em}}{2\pi}\left[e_q^2\,\frac{2.21 - 1.28z + 1.29z^2}{1 - 1.63\,\ell n\,(1-z)}\,z^{0.049} + 0.002\,(1-z)^2\,z^{-1.54}\right] \times \ell n\left(\mu^2/\mu_0^2\right). \tag{3.1}$$

The gluon-to-photon fragmentation function is

$$z\, D_{g\to\gamma}(z,\mu^2) = \frac{\alpha_{em}}{2\pi}\,0.0243\,(1-z)\,z^{-0.97}\,\ell n\left(\mu^2/\mu_0^2\right). \tag{3.2}$$

These expressions for $D_{q\to\gamma}$ and $D_{g\to\gamma}$, taken from Ref. [13], are used as a guideline for our estimates. The physical significance of scale $\mu_0$ is that the fragmentation function vanishes for energies less than $\mu_0$. For the $u, d, s$, and $c$ quarks, we set $\mu_0 = \Lambda^{(4)}_{QCD}$, as in Ref. [13]. We remark that we use simple leading order fragmentation functions in our

calculation, in contrast to the fact that we have done a next-to-leading order $\overline{\rm MS}$ calculation. It would be more consistent and, therefore, preferable to use $\overline{\rm MS}$ fragmentation functions evolved in next-to-leading order. Our choice of leading-order fragmentation functions is motivated by our desire to work with analytic expressions. In published analyses of next-to-leading order fragmentation functions, [14,15] the general formalism is presented but the fragmentation functions themselves must be obtained through numerical evolution codes. Our primary purpose in this paper is to provide a theoretical framework for the analysis of the correlated production of charm and prompt photon not necessarily to present the most up-to-date numerical predictions. Thus, we believe our leading-order fragmentation functions are adequate.

In several figures to follow, we show the predicted behavior of the photon yield as a function of $p_T^\gamma$ and $z$, as well as the breakdown of the total yield into contributions from the leading order and the various next-to-leading order pieces. The ratio $z$ is defined in Eq. (1.2). We choose to display cross sections as a function of the ratio $z$, for fixed values of $p_T^\gamma$, or as a function of $p_T^\gamma$. We choose the renormalization/fragmentation scale $\mu = p_T^\gamma$. Since both the photon and final charm particle carry large transverse momentum, we could perhaps equally well choose $\mu = p_T^c$ or some combination of the two. In selecting $p_T^\gamma$, we focus upon the photon as the "trigger" particle whose transverse momentum is well determined. We display the $\mu$ dependence of our results below.

Throughout this paper, for clarity and simplicity of the discussion, we refer consistently to charm production, e.g., $p + \bar{p} \to \gamma + c + X$. However, the numerical values of the cross sections shown in the figures are those for the sum of charm and anticharm production in $p\bar{p}$ scattering. In Fig. 3, we present the photon yield as a function of the ratio z for two choices of $p_T^\gamma$. The same results are displayed in Fig. 4 as a function of $p_T^\gamma$ for $z$ integrated over the interval 0.2 to 2.0. We restrict $z > 0.2$ as otherwise the transverse momentum of the charm quark could become unacceptably small. In Fig. 3(a), the net lowest order contribution is shown at $p_T^\gamma = 15$ GeV. The lowest order contribution is made up of the lowest order direct

term, $cg \to \gamma c$, and the fragmentation terms discussed in Sec. II.A. The direct term provides a $\delta$-function at $z = 1$ since the photon and charm quark carry equal but opposite transverse momenta at this order. The parton to photon fragmentation contributions populate the region $z > 1$. In the collinear fragmentation, the photon's transverse momentum is opposite to that of the charm quark but its magnitude is less. One of the striking features of Fig.3a, is that the net fragmentation contribution to the cross section is quite small compared to the case of inclusive photon production. At Tevatron energies, fragmentation accounts for about 50% of the inclusive yield at this value of $p_T$ [12,4]. (Note that we have not yet imposed any isolation cuts on the cross section.) One reason for the small fragmentation contribution is that fragmentation from the $cg$ initiated process is strongly suppressed due to our restriction that the charm quark and photon be in opposite hemispheres ($z \geq 0$). Thus only fragmentation from the gluon leg is included, and the $g \to \gamma$ fragmentation function is in general smaller than that for $q \to \gamma$.

In Figs. 3(b) and Fig. 3(c), we show the $z$ distribution after the next-to- leading order contributions are included. The solid lines show the full result in which both the lowest order and all next-to-leading order terms are incorporated. Comparing the solid curve in Fig. 3(b) with that in Fig. 3(a), we note that the $z$ distribution is substantially altered once the next-to-leading order terms are included. In particular, the peak at $z = 1$ is reduced in magnitude by about a factor of 2, and the $z$ distribution gains significant breadth below and above $z = 1$. The reduction in the magnitude of the peak at $z = 1$ is attributed to the effect of the $O(\alpha_s^2)$ collinear contributions on the initial parton legs. These collinear terms provide the same event structure as the lowest order direct subprocess, viz., a final-state photon and charm quark with equal but opposite transverse momenta, but their contribution is negative due to $\ln(1-z)$ terms from the phase space and large logarithms of $(1-z_{min})$ and $(z_{max}-1)$ from the $1/(1-z)_+$ and $(z-1)_+$ distributions; $z_{min}$ and $z_{max}$ are the lower and upper edges of the bins around $z = 1$. On the other hand, away from collinear configurations, the $O(\alpha_{em}\alpha_s^2)$ subprocesses, listed in Eq. (1.1), generate three body final states in which three final partons share the transverse momentum balance. The non-collinear contributions therefore populate

a broad interval in $z$.

In addition to the complete result through next-to-leading order, the solid line in Figs. 3(b) and 3(c), we display also contributions from three of the $O(\alpha_s^2)$ terms. The sum of the contributions from the other four $O(\alpha_s^2)$ terms is negligible by comparison at $p_T^\gamma = 15$ GeV. The individual contributions show the important role that the $O(\alpha_s^2)$ terms play at values of $z$ below and above 1. Contrasting Figs. 3(b) and 3(c), we see that the peak near $z = 1$ is predicted to sharpen as $p_T^\gamma$ is increased, reflecting a diminishing importance of the $O(\alpha_s^2)$ terms at larger transverse momentum.

In Fig. 4, we show the cross section as a function of the transverse momentum of the photon, $p_T^\gamma$. To obtain these results, we integrate over the interval $0.2 < z < 2.0$. These results show that the $cg$ intial state dominates the cross section until $p_T^\gamma$ approaches 100 GeV. It accounts for 60%, 55%, and 50% of total at $p_T^\gamma = 15$, 45, and 60 GeV, respectively. The $gg$ contribution is important at small values of $p_T^\gamma$, but it falls off more steeply with $p_T^\gamma$ than the $cg$ contribution. The contribution from the valence subprocess, $q\bar{q} \to c\bar{c}\gamma$, is negligible at small $p_T^\gamma$, but it overtakes the contribution of the $cg$ subprocess at sufficiently large $p_T^\gamma$. Owing to the fact the valence quarks carry significantly harder fractional momentum than the gluons and charm quarks, a major role for the valence subprocess is expected at large enough $p_T^\gamma$. However, the numerical results indicate that the hard-scattering matrix element overcomes this effect at modest values of $p_T^\gamma$, resulting in dominance of the $cg$ initial state. Comparison of Fig. (4) and Figs. 3(b) and 3(c) shows significant $z$ variation in the fraction of the total cross section accounted for by various subprocesses.

Dependence on the renormalization/factorization scale $\mu$ is displayed in Figs. 5 and 6. As $\mu$ is increased, $\alpha_s$ decreases, resulting in a reduction of the hard-scattering cross sections. The parton densities also steepen as $\mu$ is increased. Both effects contribute to the typical decrease of the cross section at fixed large $p_T^\gamma$ as $\mu$ is increased, as shown in Fig. 5. The $\mu$ dependence of the $z$ distribution presented in Fig.6 is considerably more significant. The distribution becomes more sharply peaked at $z = 1$ as $\mu$ is increased. As shown in Fig. 3(a), the leading order direct contribution produces a sharp peak at $z = 1$, whereas the next-to-

leading order contributions broaden the distribution, as shown in Figs. 3(b) and 3(c). The decrease of $\alpha_s$ as $\mu$ increases diminishes the relative importance of the next-to-leading order contributions.

The functional form of $D_{q\to\gamma}(z,\mu^2)$, Eq. (3.1), shows that the fragmentation contribution increases logarithmically as $\mu$ is increased. If the fragmentation contributions played a major role in the final answer, one would expect different $\mu$ dependence from that shown in Fig. 6.

In Fig. 7, we present the "$K$-factor" as a function of $p_T^\gamma$. Here $K$ is defined as the ratio of the complete answer through next-to-leading order to the full leading order answer (including the leading order fragmentation terms). Our results show that for $z > 0.2$, the inclusive $K$ factor is about 2 for $p_T^\gamma > 15$ GeV. In the inclusive case, no isolation requirement is imposed on the photon. To make contact with experiment, an isolation restriction is necessary. Because fragmentation contributions do not play a significant role in the associated production of photon plus charm for $z > 0.2$, we do not expect a great change of the K-factor after isolation is imposed. To estimate the impact of isolation, we use a combination of analytic and Monte Carlo methods. [16] We choose an isolation cone size $R = 0.7$, and energy resolution parameter, $\epsilon = 2\ GeV/p_T^\gamma$, as is done in the CDF experiment [1]. We find that the K-factor is reduced to about 1.5, in respectable agreement with experimental indications. [1]

## IV. CONCLUSIONS

In summary, we have computed the contributions through $O(\alpha_s^2)$ in perturbative QCD for inclusive associated production of a prompt photon and a charm quark at large values of transverse momentum in high energy hadron-hadron collisions. The next-to-leading order terms alter the expected distribution in the ratio of the magnitude of the transverse momenta of the charm quark and prompt photon in an interesting and measurable fashion. The overall cross section increases by about a factor of two after the next-to-leading terms are included. Dominance of the perturbative subprocess initiated by $gc$ scattering is preserved after the

next-to-leading terms are included, justifying use of data from $p+\bar{p} \rightarrow \gamma+c+X$ in attempts to measure the charm quark momentum density in the nucleon. However, other subprocesses are shown to account for about 50% of the cross section at currently accessible values of $p_T^\gamma$, and the "background" associated with some of these subprocesses, which are not initiated by charm quark scattering, such as in Eqs. (1.1b) and (1.1c) must be taken into account in analyses done to extract the charm density.

## V. ACKNOWLEDGMENT

We thank Dr. Bob Bailey and Dr. Stephen Mrenna for valuable discussions. This work was supported by the U.S. Department of Energy, Division of High Energy Physics, Contract W-31-109-ENG-38.

## APPENDIX A: THREE BODY CROSS SECTIONS

In this Appendix we present a fairly detailed description of the techniques for performing the 3-body phase space integrals in n dimensions. We label the momenta for the general process by $p_1 + p_2 \rightarrow k_1 + k_2 + k_3$, where $p_1$ and $p_2$ are the incoming partons, and $k_1$ and $k_2$ always label the observed photon and charm quark respectively. We integrate over the kinematic variables of $k_3$.

The calculation is performed in the rest frame of $k_2$ and $k_3$. In this frame of reference $\vec{k_2} + \vec{k_3} = 0$ .

$$\begin{aligned} s_{ij} &= (k_i + k_j)^2 \\ t_i &= (p_1 - p_i)^2 \\ u_i &= (p_2 - p_i)^2, \end{aligned} \tag{A1}$$

where $i, j = 1, 2, 3$, and $t_1 = \hat{t}$ and $u_1 = \hat{u}$, as defined in Sec. II. In terms of the momenta, the variable $z$ is

$$z = -\frac{k_1^T . k_2^T}{|k_1^T|^2} = m.k_2, \tag{A2}$$

where $m$ is a vector that depends on the choice of axes. We choose our axes in $n$ dimensions such that

$$m = \sqrt{\frac{\hat{s}}{\hat{t}\hat{u}}}\,(\sinh\chi, 0, ..., 0, \cosh\chi)\,. \tag{A3}$$

The axes are fixed and cannot be changed to simplify any phase space integrals we may encounter because, unlike the case of single inclusive particle production, we will not integrate over the full range of angles. The momenta of the particles can be parametrized in this frame as

$$\begin{aligned} p_1 &= \frac{\hat{s}v}{2\sqrt{s_{23}}}(1, 0, ..., 0, \sin\psi', \cos\psi') \\ p_2 &= \frac{\hat{s}(1 - vw)}{2\sqrt{s_{23}}}(1, 0, ..., 0, \sin\psi, \cos\psi) \end{aligned}$$

$$k_1 = \frac{\hat{s}(1-v+vw)}{2\sqrt{s_{23}}}(1,0,...,0,\sin\psi'',\cos\psi'')$$
$$k_2 = \frac{\sqrt{s_{23}}}{2}(1,0,...,0,\sin\theta_1\cos\theta_2,\cos\theta_1)$$
$$k_3 = \frac{\sqrt{s_{23}}}{2}(1,0,...,0,-\sin\theta_1\cos\theta_2,-\cos\theta_1). \tag{A4}$$

Quantities $v$ and $w$ are defined in Sec. II.

From the definition of $m$, Eq. (A3), we can derive the relationships

$$\tanh\chi = \sqrt{\frac{w(1-v)}{1-vw}}$$
$$\cos\psi = \cos\psi' = \tanh\chi$$
$$\sin\psi = -\sin\psi' = -\sqrt{\frac{1-w}{1-vw}}$$
$$\cos\psi'' = \frac{1+v-vw}{1-v+vw}\tanh\chi$$
$$\sin\psi'' = -\frac{1-v-vw}{1-v+vw}\sqrt{\frac{1-w}{1-vw}}. \tag{A5}$$

The constrained three-particle phase space is expressed as

$$PS^{(3)} = \int \frac{d^nk_1}{(2\pi)^{n-1}}\frac{d^nk_2}{(2\pi)^{n-1}}\frac{d^nk_3}{(2\pi)^{n-1}}(2\pi)^n\delta^n(p_1+p_2-k_1-k_2-k_3)$$
$$\times\delta^+(k_1^2)\delta^+(k_2^2)\delta^+(k_3^2)\delta\left(v-1-\frac{\hat{t}}{\hat{s}}\right)$$
$$\times\delta\left(w+\frac{\hat{u}}{\hat{s}+\hat{t}}\right)\delta(z-m.k_2). \tag{A6}$$

After some of the integrals are done with the aid of the $\delta$-functions, the element of phase space reduces in $n = 4-2\epsilon$ dimensions to

$$PS^{(3)} = \frac{\pi\hat{s}}{8(2\pi)^5}\left(\frac{4\pi}{\hat{s}}\right)^\epsilon\frac{v}{\Gamma(1-2\epsilon)}\left(\frac{4\pi}{\hat{s}wv(1-v)}\right)^\epsilon v^{-\epsilon}(1-w)^{-\epsilon}2\sqrt{\frac{w(1-v)}{(1-vw)}}$$
$$\times\left[\frac{1-w+4w(1-v)z(1-z)}{1-vw}\right]^{-\epsilon}\int_0^\pi d\theta_2\sin^{-2\epsilon}(\theta_2). \tag{A7}$$

In particular, we integrated over angle $\theta_1$ using the function $\delta(z-m.k_2)$ and the relation

$$z = \frac{1}{2}(1-\cos\theta_1\coth\chi), \tag{A8}$$

that can be derived from it. We are left with the task of integrating the squared matrix-elements over angle $\theta_2$.

Using relations among the Mandelstam invariants, and partial fractioning, we reduce functions involving $\theta_2$ to only a few types for all subprocesses of interest. We denote the general invariant by

$$T_i = T_{i0}(\alpha_i + \beta_i \cos\theta_2), \tag{A9}$$

where $\alpha_i$ and $\beta_i$ are functions of $\psi$, $\psi'$ and $\psi''$, and hence of $v$ and $w$; $T_{i0}$ is also a function of the latter (see Eqs. (A4) and (A5)). The combinations we must consider are

$$\frac{1}{T_i}, \quad \frac{T_j^n}{T_i}, \quad \text{and} \quad \frac{1}{T_i T_j},$$

where, $i, j, n = 1, 2, 3$. These, in turn, are all expressible in terms of two general integrals, but the form of the functions $\alpha$ and $\beta$ determines the final result, such as its singularity structure.

The two general integrals are

$$I_0[T_i] = I_0 = \int_0^\pi \sin^{-2\epsilon}\theta_2 d\theta_2 = \pi 2^{2\epsilon}\frac{\Gamma[1-2\epsilon]}{\Gamma^2[1-\epsilon]}, \tag{A10}$$

and

$$\begin{aligned} I_1[T_i] &= T_{i0}\int_0^\pi \frac{\sin^{-2\epsilon}\theta_2 d\theta_2}{T_i} = \int_0^\pi \frac{\sin^{-2\epsilon}\theta_2 d\theta_2}{(\alpha+\beta\cos\theta_2)} \\ &= \frac{\pi}{\sqrt{\alpha^2-\beta^2}}\left[\frac{4\alpha^2}{\alpha^2-\beta^2}\right]^\epsilon \frac{\Gamma[1-2\epsilon]}{\Gamma^2[1-\epsilon]}\,{}_2F_1\left(\frac{1}{2}-\epsilon, -\epsilon; 1-\epsilon; \frac{\beta^2}{\alpha^2}\right). \end{aligned} \tag{A11}$$

In terms of $I_0$, the following powers and combinations of propagators yield

$$\begin{aligned} T_i^0 &\Longrightarrow I_0, \\ T_i &\Longrightarrow T_{i0}(\alpha_i I_0), \\ T_i^2 &\Longrightarrow T_{i0}^2\left(\alpha_i^2 + \frac{\beta_i^2}{2(1-\epsilon)}\right) I_0, \\ T_i T_j &\Longrightarrow T_{i0}T_{j0}\left(\alpha_i\alpha_j + \frac{\beta_i\beta_j}{2(1-\epsilon)}\right) I_0, \\ T_i^3 &\Longrightarrow T_{i0}^3\left(\alpha_i^3 + \frac{3\alpha_i\beta_i^2}{2(1-\epsilon)}\right) I_0. \end{aligned} \tag{A12}$$

In terms of $I_1$ we obtain:

$$\begin{aligned}
&\frac{1}{T_i} \Longrightarrow \frac{1}{T_{i0}} I_1[T_i], \\
&\frac{T_j}{T_i} \Longrightarrow \frac{T_{j0}}{T_{i0}} \left( \frac{\alpha_j\beta_i - \alpha_i\beta_j}{\beta_i} I_1[T_i] + \pi \frac{\beta_j}{\beta_i} \right), \\
&\frac{T_j^2}{T_i} \Longrightarrow \frac{T_{j0}^2}{T_{i0}} \left( \left[ \frac{\alpha_j\beta_i - \alpha_i\beta_j}{\beta_i} \right]^2 I_1[T_i] + \pi \left[ \frac{2\alpha_j\beta_j\beta_i - \alpha_i\beta_j^2}{\beta_i^2} \right] \right), \\
&\frac{T_j^3}{T_i} \Longrightarrow \frac{T_{j0}^3}{T_{i0}} \left( \left[ \frac{\alpha_j\beta_i - \alpha_i\beta_j}{\beta_i} \right]^3 I_1[T_i] + \pi \left[ \frac{6\alpha_j\beta_j\beta_i(\alpha_j\beta_i - \beta_j\alpha_i) + \beta_j^3(\beta_i^2 + 2\alpha_i^2)}{2\beta_i^3} \right] \right), \\
&\frac{1}{T_iT_j} \Longrightarrow \frac{1}{T_{i0}T_{j0}} \frac{1}{\alpha_j\beta_i - \alpha_i\beta_j} (\beta_i I_1[T_i] - \beta_j I_1[T_j]).
\end{aligned} \tag{A13}$$

In order to demonstrate how the different propagators are handled in the calculation, we consider a few typical examples. We examine single propagators first, then double propagators.

### 1. Single Propagators

$$(i) \quad \frac{1}{u_2}$$

In this case $\alpha = 1 - \cos\psi\cos\theta_1$, and $\beta = -\sin\psi\sin\theta_1$.

$$\alpha^2 - \beta^2 = (\cos\theta_1 - \cos\psi)^2 = 4z^2\tanh^2\chi. \tag{A14}$$

There is a singularity at $z = 0$, but the physical condition that the photon and charm quark be in opposite hemispheres guarantees $z > 0$. The integral is therefore finite and can be treated in 4-dimensions. The result is

$$\int_0^\pi \frac{\sin^{-2\epsilon}\theta_2 d\theta_2}{u_2} = \frac{\pi}{2u_{20}} \frac{1}{\tanh\chi} \frac{1}{z}. \tag{A15}$$

The result for $t_2$ is similar. In the evaluation of $u_2$ in terms of angles, $u_{20}$ is the overall factor that does not depend on angles.

$$(ii) \quad \frac{1}{s_{12}}$$

Here $\alpha = 1 - \cos\psi'' \cos\theta_1$, and $\beta = -\sin\psi'' \sin\theta_1$.

$$\alpha^2 - \beta^2 = 4\left(z + \frac{v(1-w)}{1-v+vw}\right)^2 \tanh^2\chi. \tag{A16}$$

A singularity occurs only for negative $z$ when the photon and charm quark are exactly collinear and in the same hemisphere. We can treat this integral in 4-dimensions for the same physical reason as above, with the result

$$\int_0^\pi \frac{\sin^{-2\epsilon}\theta_2 d\theta_2}{s_{12}} = \frac{\pi}{2s_{120}} \frac{1}{\tanh\chi} \frac{1}{\left(z + \frac{v(1-w)}{1-v+vw}\right)}. \tag{A17}$$

$$(iii) \quad \frac{1}{u_3}$$

In this case $\alpha = 1 + \cos\psi\cos\theta_1$, and $\beta = \sin\psi\sin\theta_1$.

$$\alpha^2 - \beta^2 = 4(1-z)^2 \tanh^2\chi. \tag{A18}$$

There is a singularity when $z = 1$, corresponding to $k_3$ and $p_2$ being collinear. This pole must be exposed and factored into the parton distributions. The integral is

$$\int_0^\pi \frac{\sin^{-2\epsilon}\theta_2 d\theta_2}{u_3} = \frac{\pi}{2u_{30}\tanh\chi} \frac{1}{|1-z|^{1+2\epsilon}} \left[\frac{1+\tanh^2\chi(1-2z)}{\tanh\chi}\right]^{2\epsilon} \frac{\Gamma(1-2\epsilon)}{\Gamma^2(1-\epsilon)} \times {}_2F_1\left(\frac{1}{2}-\epsilon, -\epsilon; 1-\epsilon; \frac{\beta^2}{\alpha^2}\right). \tag{A19}$$

This integral can be reduced if we use the expansion

$$\frac{1}{|1-z|^{1+2\epsilon}} = \frac{1}{-2\epsilon}\delta(1-z) + \frac{\theta(1-z)}{(1-z)_+} + \frac{\theta(z-1)}{(z-1)_+} - 2\epsilon\left(\frac{\ln(1-z)}{1-z}\right)_+ \theta(1-z) + O(\epsilon^2), \tag{A20}$$

and note that the hypergeometric function at $z = 1$ reduces to $2^{-2\epsilon}$. We introduce a plus-distribution,

$$\int_1^{z_{max}} \frac{f(z)}{(z-1)_+} dz = \int_1^{z_{max}} \frac{f(z) - f(1)}{(z-1)} dz, \tag{A21}$$

where $z_{max} = 1/2(1 + \coth\chi)$ from Eq. (A8). When the phase space factor involving $z$ is included in the expansion, the integral reduces to

$$\int_0^\pi \frac{\sin^{-2\epsilon}\theta_2 d\theta_2}{u_3} = \frac{\pi}{2u_{30}\tanh\chi}\frac{\Gamma(1-2\epsilon)}{\Gamma^2(1-\epsilon)}\left[\delta(1-z)\left(-\frac{1}{\epsilon}-\ln z_{max}\right)+\frac{\theta(1-z)}{(1-z)_+}+\frac{\theta(z-1)}{(z-1)_+}\right]. \tag{A22}$$

The result for $1/t_3$ is similar.

$$(iv) \quad \frac{1}{s_{13}}$$

This propagator occurs when there is a quark $k_3$ in the final state that may become collinear with the photon $k_1$, such as in Eqs. (1.1b)-(1.1g). Here, $\alpha = 1+\cos\psi''\cos\theta_1$, and $\beta = \sin\psi''\sin\theta_1$.

$$\alpha^2-\beta^2 = 4\left(z-\frac{1}{1-v+vw}\right)^2\tanh^2\chi. \tag{A23}$$

There is a singularity at $z = 1/(1-v+vw) = z_1$. Using an expansion similar to that in Eq. (A20), but with $(1-z)$ and $(z-1)$ replaced by $(z_1-z)$ and $(z-z_1)$, we cast the result in the form

$$\int_0^\pi \frac{\sin^{-2\epsilon}\theta_2 d\theta_2}{s_{13}} = \frac{\pi}{2s_{130}\tanh\chi}\frac{\Gamma(1-2\epsilon)}{\Gamma^2(1-\epsilon)}\left[\delta(z-z_1)\left(-\frac{1}{\epsilon}-\ln\left(1-\frac{z_{min}}{z_1}\right)\right)\right.$$
$$\left.+\frac{\theta(z_1-z)}{(z_1-z)_+}+\frac{\theta(z-z_1)}{(z-z_1)_+}\right]. \tag{A24}$$

Here $z_{min} = 1/2(1-\coth\chi)$, and the plus-distributions are defined in a similar way, but with limits from 0 to $z_1$ and $z_1$ to $z_{max}$.

In this outline, we have omitted phase space factors present in Eq. (A7) and included them only when they are important for the expansions performed. In principle, all phase space factors should be included and, for example, $v^\epsilon$ would be expanded as

$$1-\epsilon\ln(v)+\frac{\epsilon^2}{2}\ln^2(v)$$

and combined with the final results of $(i)$ to $(iv)$ above, before $\epsilon$ is set to zero. Factors such as $2v\tanh\chi$ have also been omitted but are included in our final results.

### 2. Double Propagators

We examine a few important examples of double propagators. Some have been calculated previously, [6,8] but there are cases not encountered in earlier calculations that we stress here. We include all phase space factors since most are needed in the expansions.

$$(i) \quad \frac{1}{t_3 u_3}$$

This double pole propagator was encountered in Ref. [6]. The result is

$$\begin{aligned}
\int_0^\pi \frac{\sin^{-2\epsilon}\theta_2 d\theta_2}{t_3 u_3} = & \frac{\pi v^{1-\epsilon}}{t_{30} u_{30}} \frac{\Gamma(1-2\epsilon)}{\Gamma^2(1-\epsilon)} \\
& \times \Bigg[ (1-vw) \left( \frac{\theta(1-z)}{(D_1(1-z))_+} + \frac{\theta(z-1)}{(D_1(z-1))_+} \right) \\
& + \delta(1-z) \left( -\frac{1-vw}{1-w} \ln\left( \frac{\tanh\chi + \coth\chi}{2} \right) \right. \\
& + v \left. \left( -\frac{1}{\epsilon} - \ln(1-vw) + 2\ln(1-w) \right) \right) \\
& - (1-v) \left( \left( \frac{1}{\epsilon} + \ln(1-v) \right) \frac{1}{(1-w)_+} \right. \\
& - 2 \left( \frac{\ln(1-w)}{(1-w)} \right)_+ + \frac{1}{1-w} \ln\left( \frac{1-vw}{1-w} \right) \Bigg) \\
& + \delta(1-z)\delta(1-w) \left( \frac{1}{2\epsilon^2} + \frac{1}{2\epsilon} \ln(1-v) + \frac{1}{4} \ln^2(1-v) \right) (1-v) \Bigg], \qquad \text{(A25)}
\end{aligned}$$

where $D_1 = 1 - w + 2(1-z)w(1-v)$.

$$(ii) \quad \frac{1}{t_3 u_2}$$

Applying the last result in Eq. (A13), we get a term $1/(1-2z)$ multiplying the integrals for the propagators $(\beta(u_2)I[u_2] + \beta(t_3)I[t_3])$, along with other factors. This term is singular at $z = 1/2$, but the singularity has no physical origin and must be removed before numerical evaluation of the cross section. The integral of $1/u_2$ yields a term $1/z$ (Eq. (A15)) while that of $t_3$ yields plus-distributions in $(1-z)$ and $(z-1)$ (Eq. (A22)). To remove the false singularity we make the replacement

$$\frac{1}{z} \to \frac{\theta(1-z)}{z} + \frac{\theta(z-1)}{z}.$$

These $\theta$ functions can be combined with the plus-distributions from the second term in $(\beta(u_2)I[u_2] + \beta(t_3)I[t_3])$ to produce

$$\int_0^\pi \frac{\sin^{-2\epsilon}\theta_2 d\theta_2}{t_3 u_2} = \frac{\pi v^{1-\epsilon}(1-w)^{-\epsilon}}{2t_{30}u_{20}\tanh^2\chi}\frac{\Gamma(1-2\epsilon)}{\Gamma^2(1-\epsilon)}\left[\delta(1-z)\left(-\frac{1}{\epsilon}-\ln z_{max}\right)+\frac{\theta(1-z)}{z(1-z)_+}\right.$$
$$\left. +\ \theta(z-1)\left(\frac{1}{(z-1)_+}+\frac{1+2z}{(1-2z)z}\right)\right]. \tag{A26}$$

The term $1/(1-2z)$ is harmless when multiplied by $\theta(z-1)$.

$$(iii)\quad \frac{1}{t_3 s_{23}}$$

This case involves singularities when $z \to 1$ and $w \to 1$. It is discussed in Ref. [8]. The result is

$$\int_0^\pi \frac{\sin^{-2\epsilon}\theta_2 d\theta_2}{t_3 s_{23}} = \frac{\pi v^{1-\epsilon}}{\hat{s}vt_{30}}\frac{\Gamma(1-2\epsilon)}{\Gamma^2(1-\epsilon)}\left[-\frac{1}{\epsilon}\delta(1-w)\left(-\frac{1}{\epsilon}\delta(1-z)+\theta(1-z)\left(\frac{1}{(1-z)_+}\right.\right.\right.$$
$$\left.\left.\left. -\ \epsilon\frac{\ln(z)}{1-z}-\epsilon\left(\frac{\ln(1-z)}{1-z}\right)_+\right)\right)+\frac{1}{(1-w)_+}\left(-\frac{1}{\epsilon}\delta(1-z)+\frac{\theta(1-z)}{(1-z)_+}\right)\right.$$
$$\left. +\ \frac{1}{1-w}\left(\frac{\theta(z-1)}{(z-1)_+}-\delta(1-z)\ln(z_{max})\right)+\left(\frac{\ln(1-w)}{1-w}\right)_+\right]. \tag{A27}$$

A similar result is obtained for $1/(s_{23}u_3)$ and for $1/(s_{23}s_{13})$ except that, in the latter case, the singularities occur at $w \to 1$ and $z \to z_1$.

Finally, since $s_{23} = \hat{s}v(1-w)$, we make the point that in other cases when the propagator $1/s_{23}$ occurs in the denominator of the matrix elements, it must be combined with the phase space factor $(1-w)^{-\epsilon}$ and expanded via

$$(1-w)^{-1-\epsilon} = -\frac{1}{\epsilon}\delta(1-w)+\frac{1}{(1-w)_+}+\epsilon\left(\frac{\ln(1-w)}{1-w}\right)_+ + O(\epsilon). \tag{A28}$$

The results of this expansion are combined with the phase space factor in Eq. (A7). To ensure in every case that we retain all finite terms and obtain the correct result in the limit when $k_2$ and $k_3$ become collinear, we always make the full replacement

$$\int_0^\pi \frac{\sin^{-2\epsilon}\theta_2 d\theta_2}{s_{23}} = \frac{2^{1+2\epsilon}\pi\tanh\chi v^{-\epsilon}}{\hat{s}}\frac{\Gamma(1-2\epsilon)}{\Gamma^2(1-\epsilon)}\left[(1-z)\left(-\frac{1}{\epsilon}\delta(1-w)\left(-\frac{1}{\epsilon}\delta(1-z)\right.\right.\right.$$
$$\left.\left.\left. +\ \theta(1-z)\left(\frac{1}{(1-z)_+}-\epsilon\frac{\ln(z)}{1-z}-\epsilon\left(\frac{\ln(1-z)}{1-z}\right)_+\right)\right)\right)\right.$$
$$\left. +\ \frac{1}{(1-w)_+}\left(-\frac{1}{\epsilon}\delta(1-z)+\frac{\theta(1-z)}{(1-z)_+}\right)+\delta(1-z)\left(\frac{\ln(1-w)}{1-w}\right)_+\right]. \tag{A29}$$

Most of these terms will vanish since, for example, $(1-z)$ will usually multiply $\delta(1-z)$ and $(1-w)$ will multiply $\delta(1-w)$. In a few special cases, as when there is a $P_{qq}$ splitting function in the collinear limit, as is the case when the final-state gluon becomes parallel to the $c$-quark in the $cg$ initiated process, the full expansion is needed in order to expose the singularity. This singularity may then be factored into the $c$-quark fragmentation function.

# REFERENCES


[1] CDF Collaboration, R. Blair *et al*, FERMILAB-Conf-95/245-E, to be published in the Proceedings of the 10th Topical Workshop on Proton-Antiproton Collider Physics, FNAL, May, 1995.

[2] P. Nason, S. Dawson, and R.K. Ellis, Nucl. Phys. **B303**, 607 (988); **B327**, 49 (1989); Erratum: **B335**, 260 (1990); W. Beenakker, H. Kuijf, W.L. van Neerven, and J. Smith, Phys. Rev. **D40**, 54 (1989); W. Beenakker, W.L. van Neerven, R. Meng, G.A. Schuler, and J. Smith, Nucl. Phys. **B351**, 507 (1991); E. L. Berger and R. Meng, Phys. Rev. **D49** 3248, (1994), and references therein.

[3] P. Aurenche *et al*, Phys Lett. **140B**, 87 (1984); P. Aurenche *et al*, Nucl. Phys. **B297**, 661 (1988); A. P. Contogouris, S. Papadopoulos, and D. Atwood, Theor. Math. Phys. **87**, 374 (1991); H. Baer, J. Ohnemus, and J. F. Owens, Phys. Rev. **D42**, 61 (1990).

[4] L. E. Gordon and W. Vogelsang, Phys. Rev. **D48**, 3136 (1993) and **D50**, 1901 (1994); M. Glück, L. E. Gordon, E. Reya, and W. Vogelsang, Phys. Rev. Lett. **73**, 388 (1994).

[5] E. L. Berger and J.-W. Qiu, Phys. Lett. **B248**, 371 (1990); and Phys. Rev. **D44**, 2002 (1991).

[6] P. Aurenche, A. Douiri, R. Baier, M. Fontannaz, and D. Schiff, Z. Phys. **C29**, 459 (1985).

[7] B. Bailey, J.Ohnemus, and J.F.Owens, Phys. Rev. **D46**, 2018 (1992).

[8] P. Aurenche, A. Douiri, R. Baier, M. Fontannaz, and D. Schiff, Z. Phys. **C24**, 309 (1984).

[9] E. L. Berger, Phys. Rev. **D37**, 1810 (1988); M. Mangano, P. Nason, and G. Ridolfi Nucl. Phys. **B373**, 295 (1992).

[10] S. D. Ellis, Z. Kunszt, and D. E. Soper, Phys. Rev. Lett. **69**, 1496 (1992); W. T. Giele,

E. W. N. Glover, and D. A. Kosower, Phys. Rev. Lett. **73**, 2019 (1994); S. D. Ellis and D. E. Soper, Phys. Rev. Lett. **74**, 5182 (1995).

[11] E. L. Berger *et al*, Phys. Rev. **D40**, 83 (1989); U. Baur *et al*, Phys. Lett. **B318**, 544 (1993).

[12] E. L. Berger, E. Braaten, and R. D. Field, Nucl. Phys. **B239**, 52 (1984).

[13] D.W. Duke and J. F. Owens, Phys. Rev. **D26**, 1600 (1982); J. F. Owens, Rev. Mod. Phys. **59**, 465 (1987).

[14] P. Aurenche *et al*, Nucl. Phys. **B399**, 34 (1993).

[15] M. Glück, E. Reya, and A. Vogt, Phys. Rev. **D48**, 116 (1993).

[16] B. Bailey, E. L. Berger, and L. E. Gordon, Argonne report ANL-HEP-PR-95-87, to be published.

[17] M. Stratmann and W. Vogelsang, Phys. Rev. **D52**, 1535 (1995).

[18] R. K. Ellis, M. A. Furman, H. E. Haber, and I. Hinchliffe, Nucl. Phys. **B173**, 397 (1980).

[19] G. Altarelli and G. Parisi, Nucl. Phys. **B126**, 298 (1977).

[20] M. Glück, E. Reya, and A. Vogt, Phys. Rev. **D45**, 3986 (1992).

[21] H. L. Lai *et al*, CTEQ Collaboration, Phys. Rev. **D51**, 4763 (1995).

[22] S. J. Brodsky, P. Hoyer, C. Peterson, and N. Sakai, Phys. Lett. **B93**, 451 (1980); S. J. Brodsky, C. Peterson, and N. Sakai, Phys. Rev. **D23**, 2745 (1981).

**Figure Captions**

[1] (a) Lowest order Feynman diagrams for $\gamma$ plus $c$ quark production; $k_1$ and $k_2$ are the four-vector momenta of the photon and charm quark. (b) Examples of virtual corrections to the lowest order diagrams. (c) Examples of next-to-leading order three-body final-state diagrams for the $gc$ initial state.

[2] Charm quark density $c(x, Q)$ as a function of Bjorken $x$ at $Q = 10$ GeV. The solid line shows the expectation of the GRV parton densities [20], and the dotted line that of the the CTEQ3M densities [21].

[3] Cross section $d\sigma/dp_T^\gamma dy^\gamma dz$ as a function of $z$ for $p + \bar{p} \to \gamma + c + X$ at $\sqrt{s} = 1.8$ TeV. We set $y^\gamma = 0$. Results are presented in the form of a histogram in bins of width $\Delta z = 0.2$. In (a), for $p_T^\gamma = 15$ GeV, we show the net contribution from the lowest order direct process $gc \to \gamma c$ and from all the leading order fragmentation processes $p_1 p_2 \to p_3 c$ followed by the collinear fragmentation $p_3 \to \gamma X$. In (b) and (c), for $p_T^\gamma$ =15 and 45 GeV, respectively, we display the full cross section through next-to-leading order (solid line) and contributions from three important $O(\alpha_s^2)$ subprocesses.

[4] The transverse momentum dependence of $d\sigma/dp_T^\gamma dy^\gamma dz$, for $z$ integrated over the interval $0.2 < z < 2.0$. The upper solid line shows the sum of all subprocesses through next-to-leading order. The dashed line shows the sum of the $O(\alpha_s)$ and $O(\alpha_s^2)$ contributions from the $cg$ initial state. The $O(\alpha_s^2)$ contributions from the $gg$ and $cq$ initial states are shown as dash-dot and dotted curves. The lower solid line shows the $O(\alpha_s^2)$ contribution from the $\bar{q}q$ (and $\bar{c}c$ and $cc$) initial state.

[5] The renormalization/factorization scale $\mu$ dependence. For the sum of all contributing subprocesses, $d\sigma/dp_T^\gamma dy^\gamma dz$, for $y^\gamma = 0$ and $z$ integrated over the interval $0.2 < z < 2.0$, is shown as a function of $p_T^\gamma$ for three values of $\mu/p_T^\gamma$: 0.5, 1.0, and 2.

[6] The renormalization/factorization scale $\mu$ dependence of $d\sigma/dp_T^\gamma dy^\gamma dz$. Results are shown as a function of $z$ at $p_T^\gamma = 20$ GeV for three values of $\mu/p_T^\gamma$: 0.5, 1.0, and 2.

[7] The K factor defined in the text is shown as a function of $p_T^\gamma$ for inclusive (i.e., non-isolated) photons (solid line) and isolated photons (dashed line); $y^\gamma = 0$ and $0.2 < z < 2.0$.


(a)

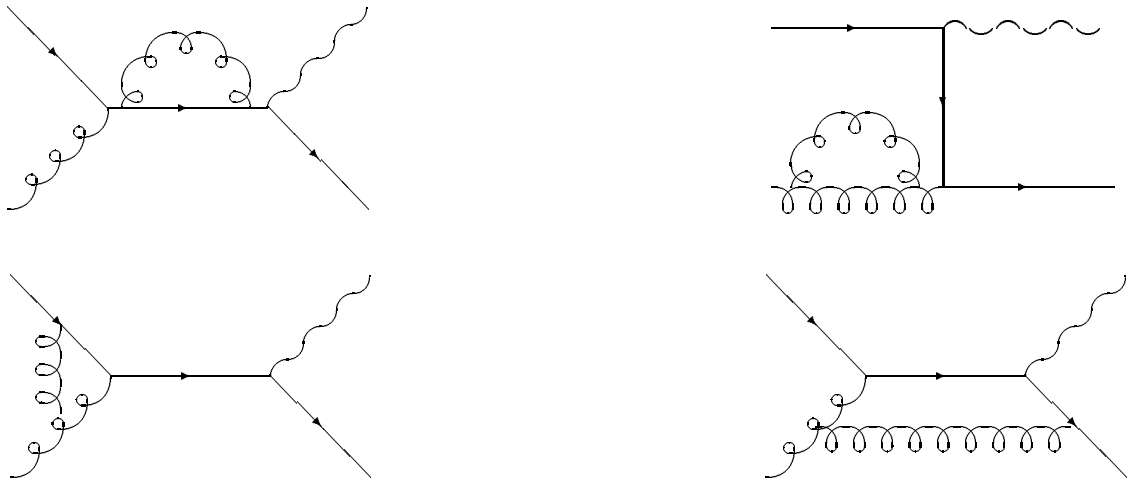

(b)

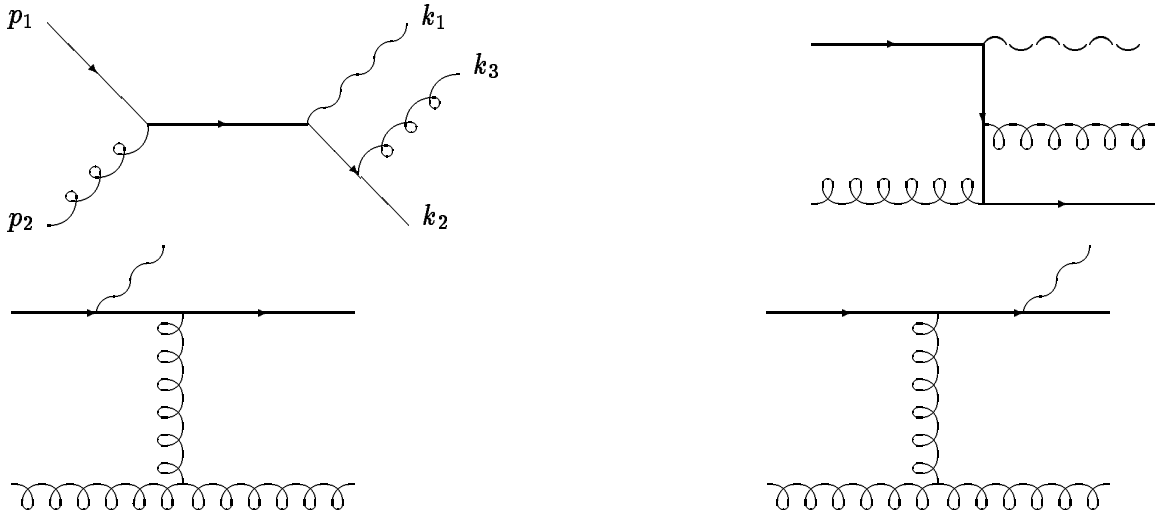


(c)

Fig.1

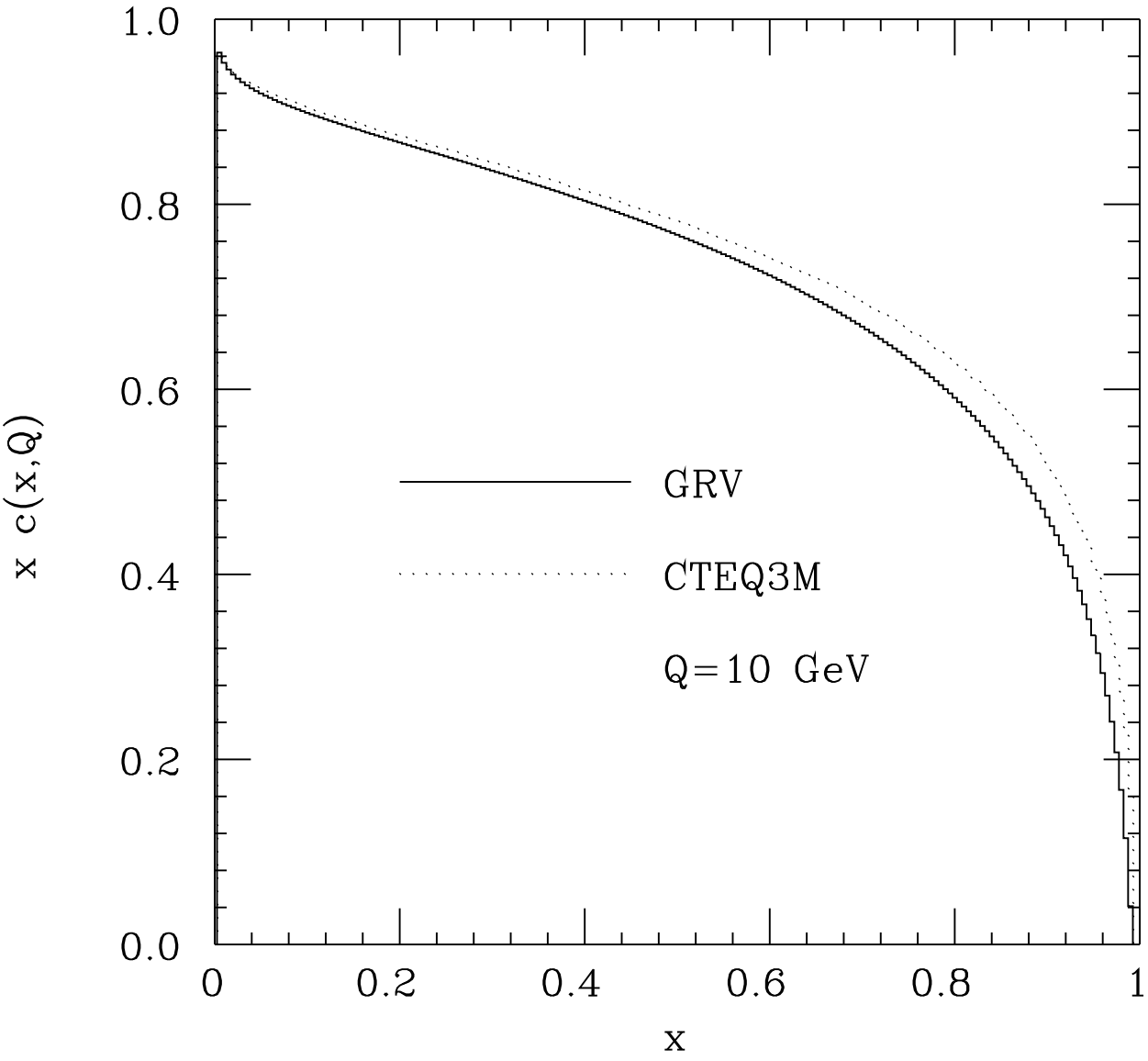


Fig. 2

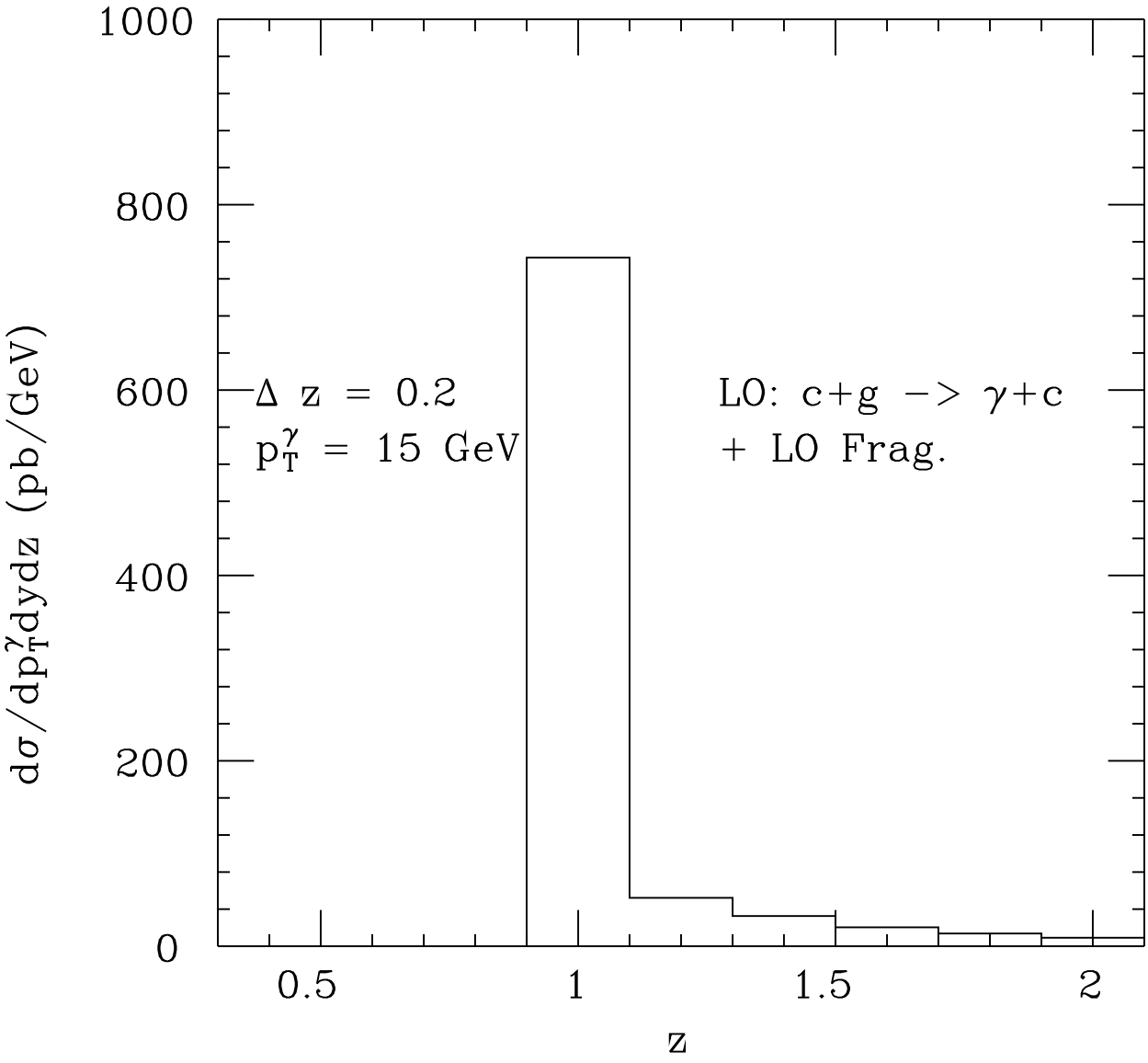
1000
800
600
400
200
0
0.5
1
1.5
2
z
dσ/dp$_T^\gamma$dydz (pb/GeV)
Δ z = 0.2
p$_T^\gamma$ = 15 GeV
LO: c+g −> γ+c
+ LO Frag.

Fig. 3a

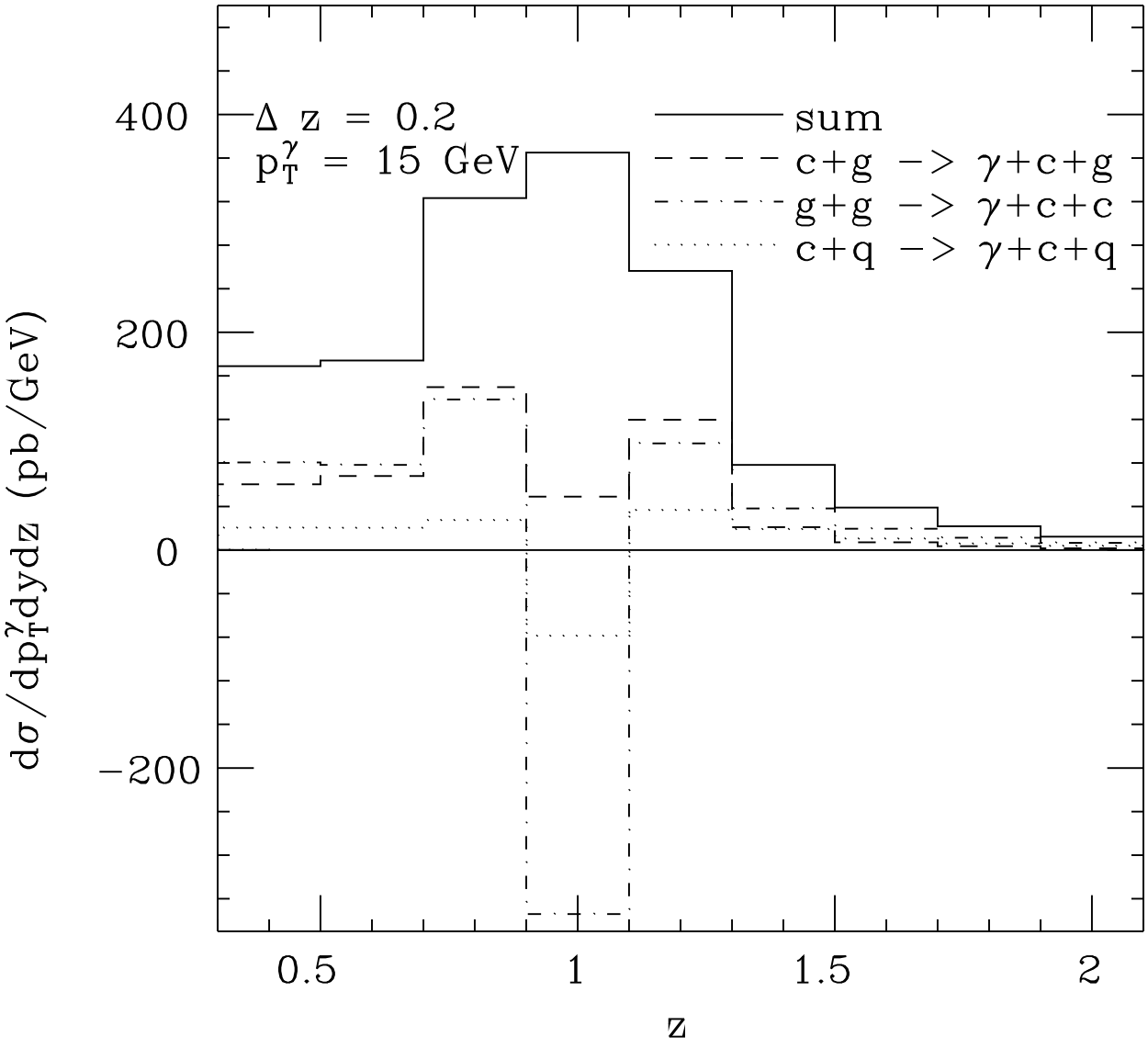
400
200
0
−200
0.5
1
1.5
2
z
dσ/dp$_T^\gamma$dydz (pb/GeV)
Δ z = 0.2
p$_T^\gamma$ = 15 GeV
sum
c+g −> γ+c+g
g+g −> γ+c+c
c+q −> γ+c+q

Fig. 3b

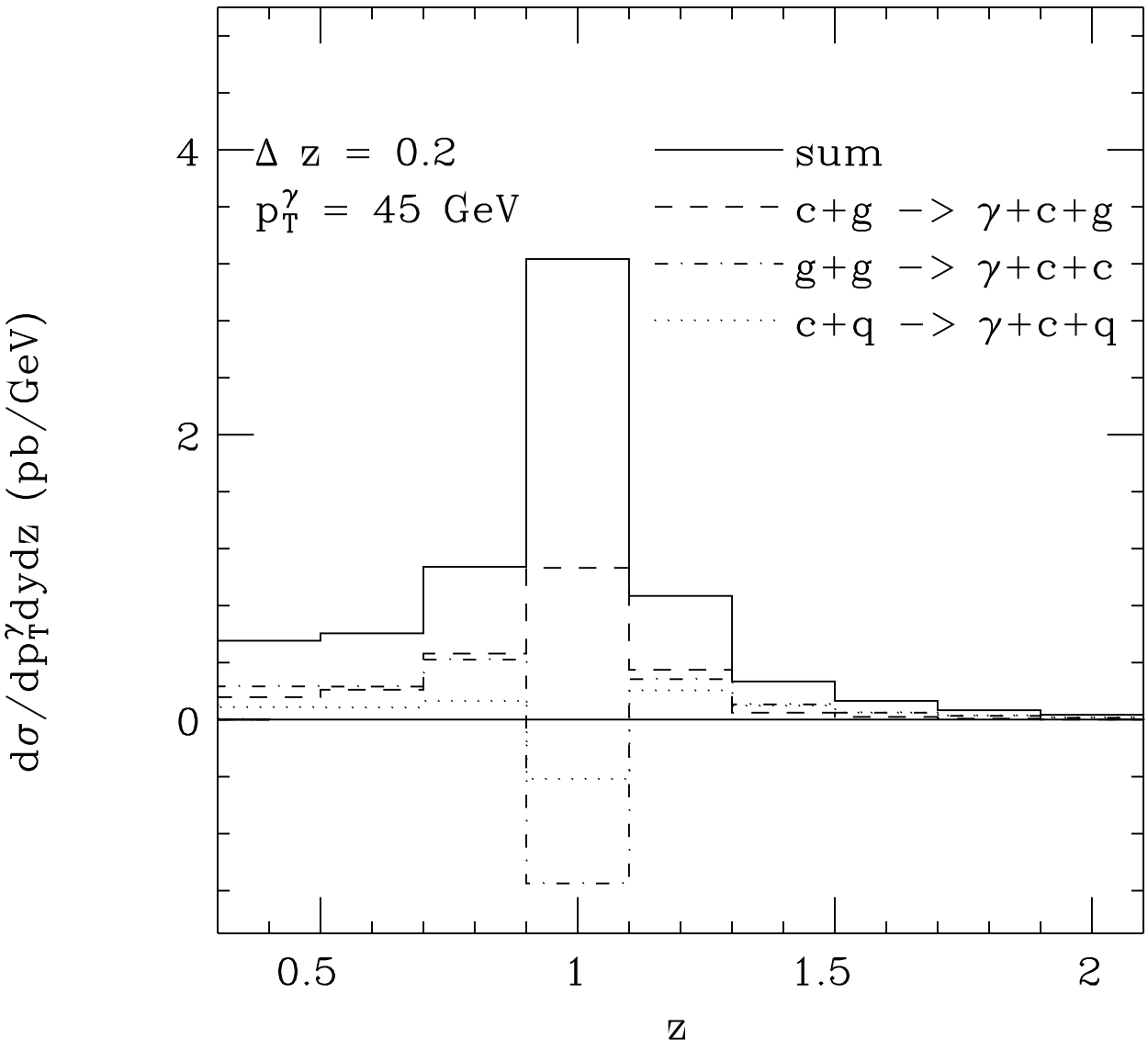
Δ z = 0.2
$p_T^\gamma$ = 45 GeV
sum
c+g -> γ+c+g
g+g -> γ+c+c
c+q -> γ+c+q
dσ/dp$_T^\gamma$dydz (pb/GeV)
z
0
2
4
0.5
1
1.5
2

Fig. 3c

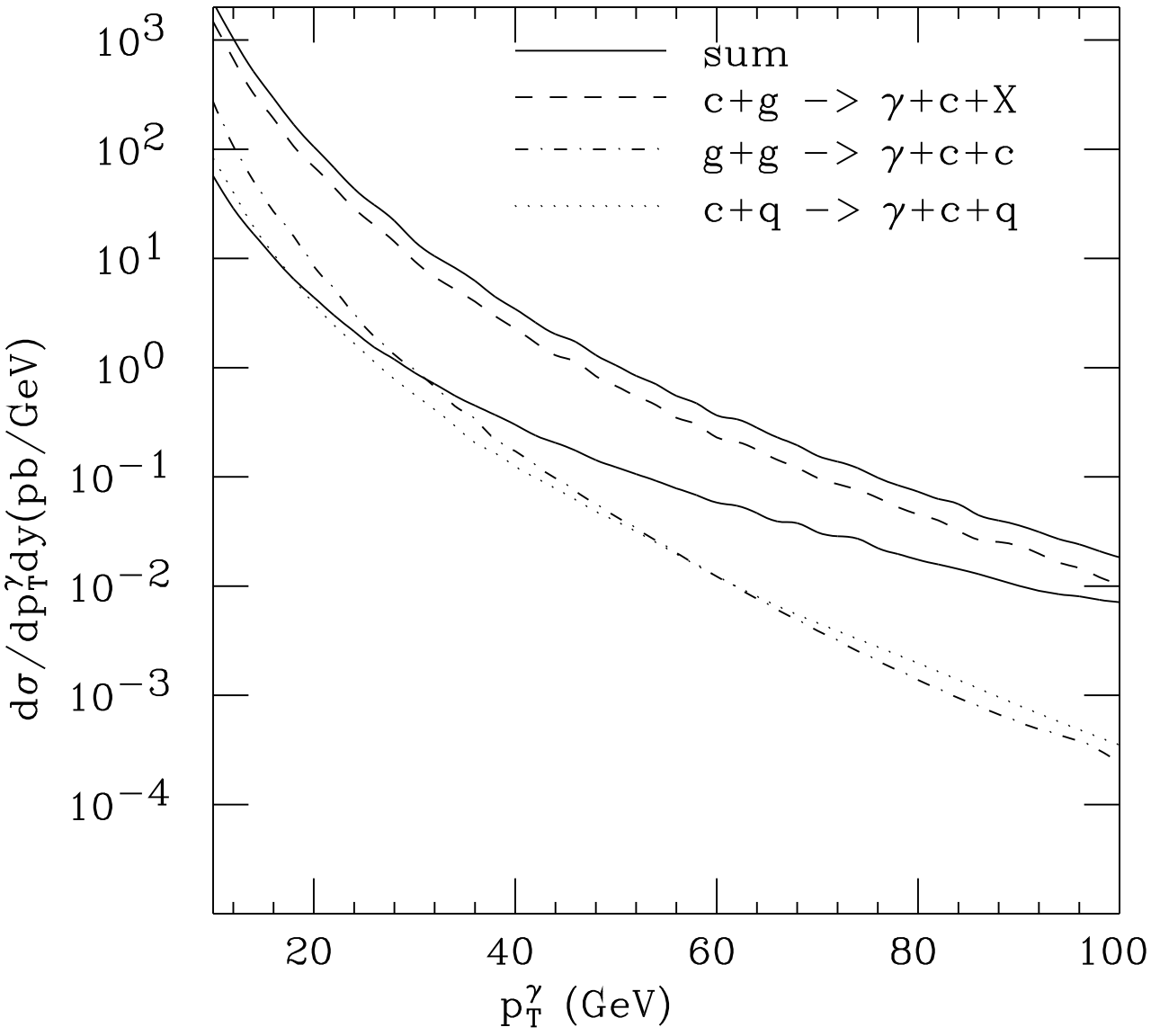
sum
c+g -> γ+c+X
g+g -> γ+c+c
c+q -> γ+c+q
dσ/dp_T^γdy(pb/GeV)
10^3
10^2
10^1
10^0
10^-1
10^-2
10^-3
10^-4
20
40
60
80
100
p_T^γ (GeV)

Fig. 4

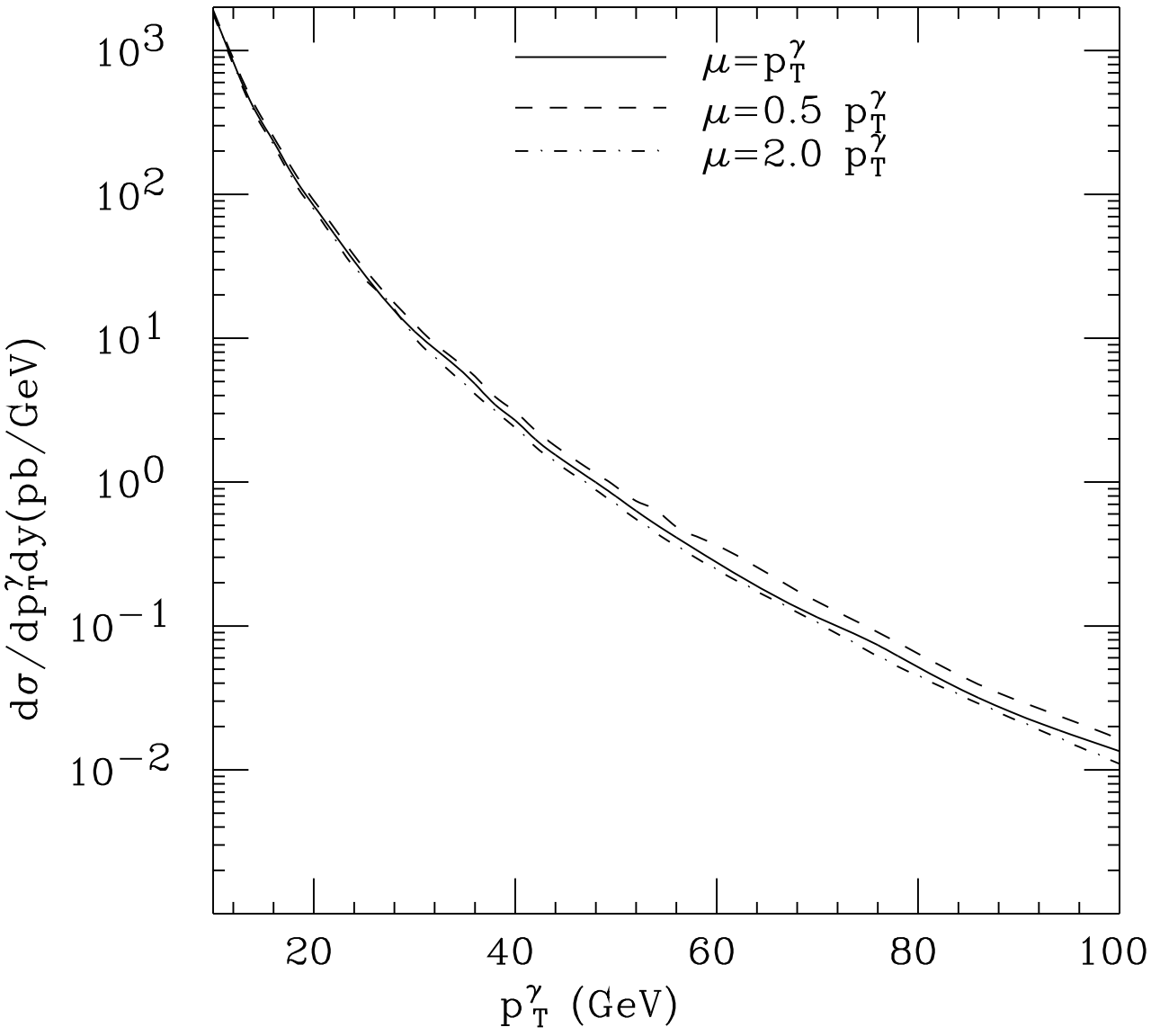
$10^3$
$10^2$
$10^1$
$10^0$
$10^{-1}$
$10^{-2}$
$d\sigma/dp_T^\gamma dy$(pb/GeV)
$\mu=p_T^\gamma$
$\mu=0.5\ p_T^\gamma$
$\mu=2.0\ p_T^\gamma$
20
40
60
80
100
$p_T^\gamma$ (GeV)

Fig. 5

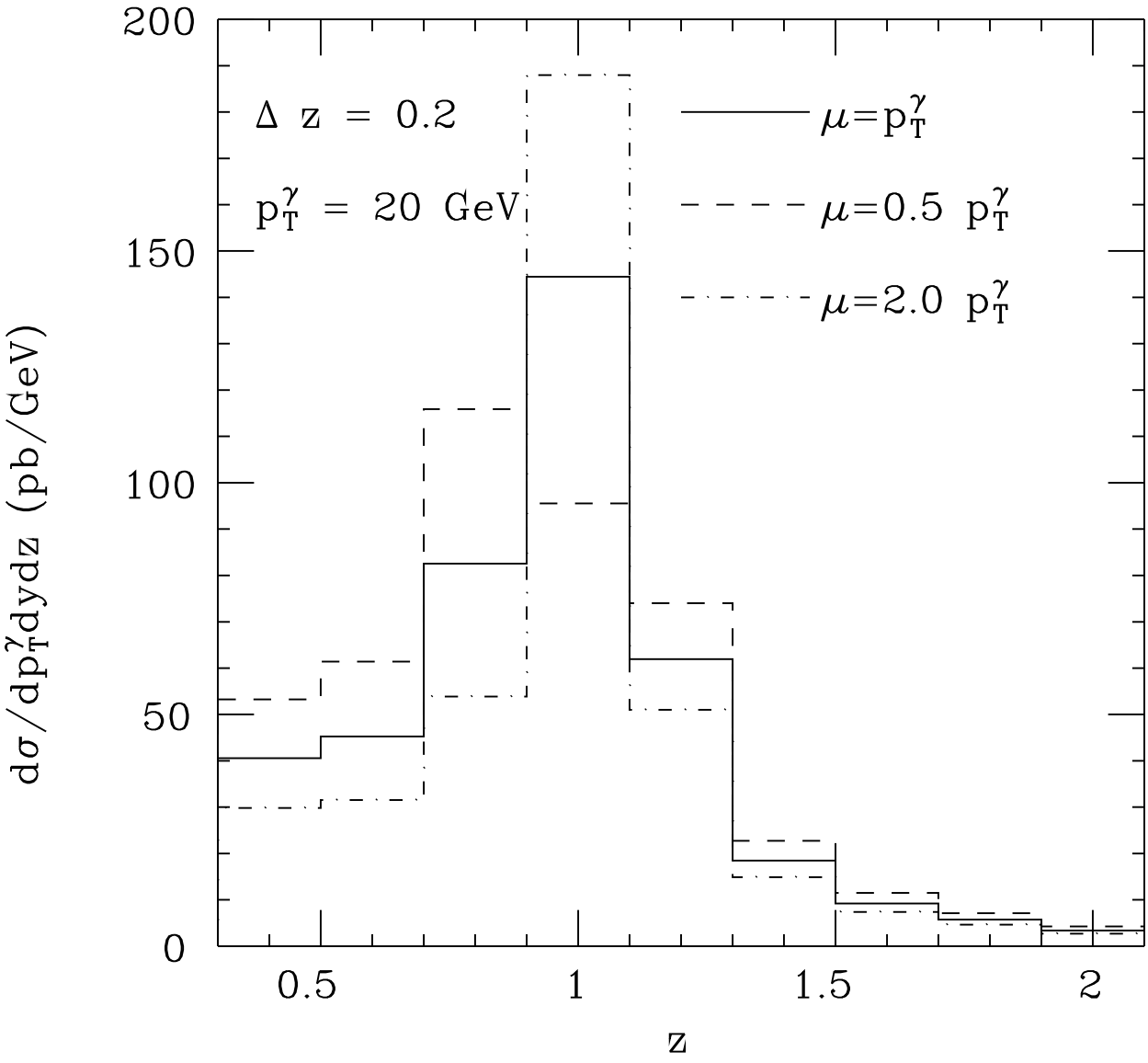
200
150
100
50
0
0.5
1
1.5
2
z
dσ/dp$_T^\gamma$dydz (pb/GeV)
Δ z = 0.2
p$_T^\gamma$ = 20 GeV
μ=p$_T^\gamma$
μ=0.5 p$_T^\gamma$
μ=2.0 p$_T^\gamma$

Fig. 6

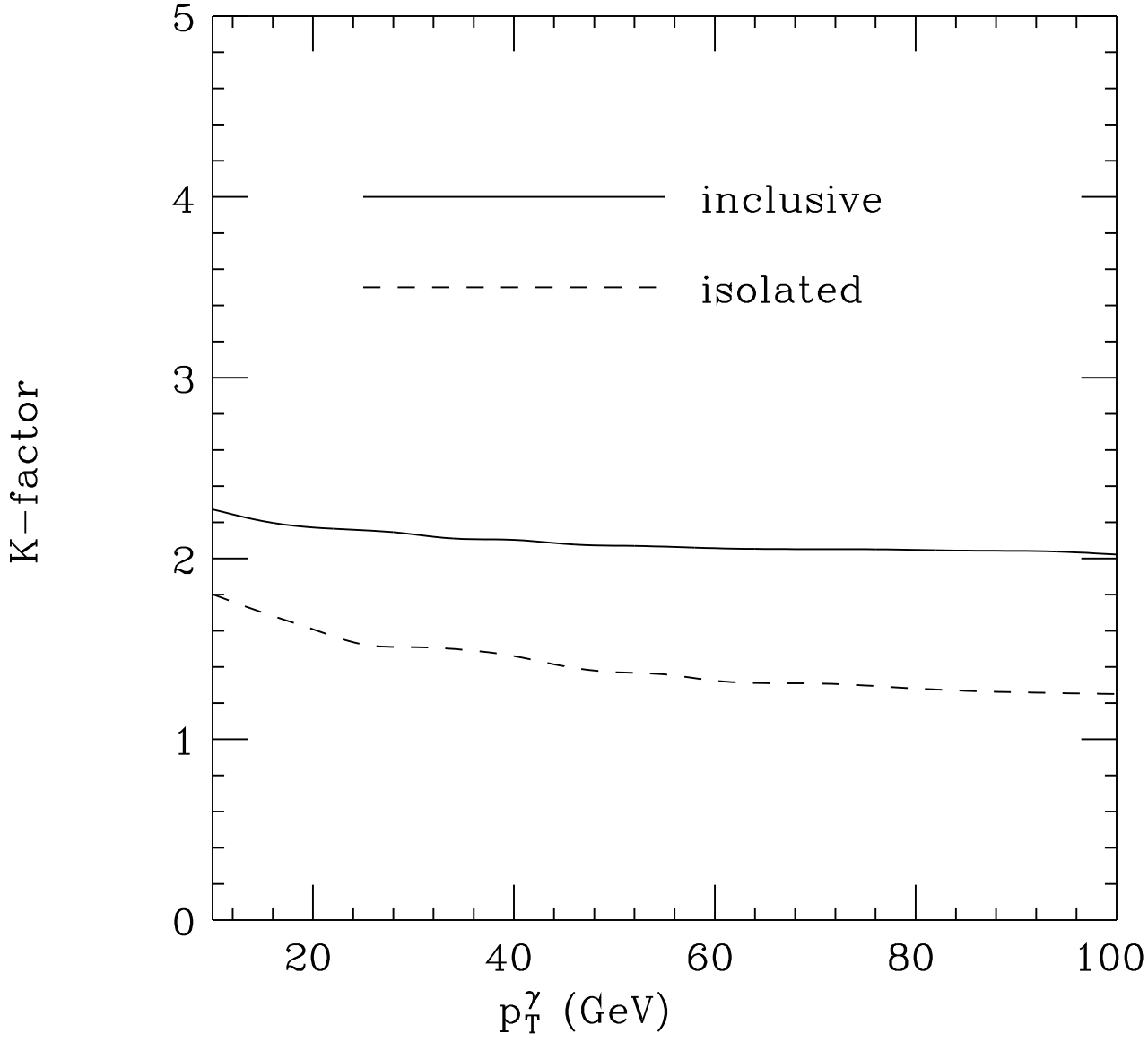
5
4
3
2
1
0
K-factor
inclusive
isolated
20
40
60
80
100
$p_T^\gamma$ (GeV)

Fig. 7